fractal and fractional

MDPI

Article

NMR-Based Fractal Characterization of Capillary-Force-Regulated Shut-in Imbibition in Continental Shale Oil: Pore-Size-Dependent Recovery, Nanopore Mobilization Threshold, and Permeability Enhancement

Hui Li and Ben Li *

State Key Laboratory of Petroleum Resources and Engineering, China University of Petroleum (Beijing), Beijing 102249, China
* Correspondence: benli@cup.edu.cn

Abstract

Continental shale oil reservoirs contain multiscale pore–fracture systems with strong heterogeneity and fractal characteristics, which complicate oil mobilization during post-fracturing shut-in imbibition. In this study, shale cores from the LGS Formation (a lacustrine continental shale oil formation in China) were used to investigate capillary-force-regulated pressurized shut-in imbibition by integrating interfacial tension measurements, apparent contact angle tests, capillary pressure calculation, time-lapse nuclear magnetic resonance (NMR), NMR-based fractal characterization, visual observations, and pre-/post-imbibition permeability measurements. Two surfactant-based imbibition agents with different capillary-force regulation mechanisms were compared to represent different capillary-force regulation pathways. Agent 1 mainly modified apparent wettability, increasing the contact angle from 51.0° to 66.1°, whereas Agent 2 reduced the oil–water interfacial tension from 31.85 to 22.12 mN/m while maintaining a favorable apparent contact angle of 49.3°. Time-lapse NMR results showed that oil recovery increased with shut-in time and reached approximately 12–30% after 144 h. Agent 2 generally produced higher recovery than Agent 1, with the optimum response at 0.15 wt%. NMR-derived fractal dimensions ranged mainly from 2.32 to 2.61, confirming the multiscale heterogeneity of the LGS shale pore system. Pore-size-resolved recovery further showed that oil mobilization was dominated by pores larger than 20 nm and microfracture-related spaces, whereas pores smaller than 20 nm contributed only limited bulk recovery. This indicates an apparent nanopore mobilization threshold near 20 nm, controlled by fractal pore complexity, pore-throat connectivity, oil adsorption, capillary pressure, and molecular accessibility of imbibition agents. Visual and permeability evidence further showed that pressurized imbibition can selectively activate connected pore–fracture pathways. Post-imbibition dry-core permeability increased in all tested samples, although the enhancement was highly heterogeneous. These results demonstrate that shut-in imbibition in LGS shale is governed by coupled interfacial regulation, fractal pore heterogeneity, pore-size-dependent oil accessibility, and selective pore–fracture structural modification.

Keywords: continental shale oil; NMR-based fractal characterization; shut-in imbibition; capillary-force regulation; pore-size-dependent recovery; nanopore mobilization threshold; permeability enhancement

Check for updates

Academic Editor: Frits Agterberg

Received: 4 June 2026
Revised: 30 June 2026
Accepted: 9 July 2026
Published: 16 July 2026

Copyright: © 2026 by the authors. Licensee MDPI, Basel, Switzerland. This article is an open access article distributed under the terms and conditions of the Creative Commons Attribution (CC BY) license.

1. Introduction

Continental shale oil has become an important unconventional resource, particularly in lacustrine shale systems where organic-rich mudstones, laminated fabrics, nanoscale pore-throat networks, and bedding-related discontinuities jointly control hydrocarbon storage and recovery. In China, lacustrine shale oil systems are characterized by strong lithofacies heterogeneity, complex oil occurrence states, fine pore-throat systems, and pronounced geological variability [1]. Recent studies have further emphasized that continental shale oil movability is controlled not only by total organic carbon and thermal maturity, but also by pore structure, oil occurrence state, mineral composition, and pore–fracture connectivity [2]. Compared with conventional reservoirs, continental shale oil reservoirs commonly contain organic pores, inorganic nanopores, intergranular pores, clay-related pores, bedding-parallel voids, and microfractures, producing a broad pore-size spectrum from nanometer-scale storage pores to micrometer-scale connected flow pathways [3]. The morphology and connectivity of nanopores in mudrocks have been shown to exert a strong control on hydrocarbon storage and transport [4]. In particular, low nanopore connectivity can restrict effective fluid production even when abundant nanopore storage space exists [5].

Bedding and microfractures further complicate fluid transport in shale. Bedding-related anisotropy can generate direction-dependent permeability, fracture propagation, and fluid accessibility. Early work has shown that sedimentary bedding can be an important cause of permeability anisotropy in porous rocks [6]. In shale reservoirs, lamination, natural fractures, and bedding-parallel discontinuities may create preferential flow pathways along bedding while also restricting cross-bedding transport [7]. X-ray tomography studies have demonstrated that clay-rich mudstones can contain highly anisotropic and tortuous permeable pathways [8]. Three-dimensional microfracture characterization has also shown that shale microfractures are spatially heterogeneous and can strongly influence connected flow capacity [9]. Therefore, shale oil recovery after hydraulic fracturing should be interpreted within a multiscale pore–fracture framework rather than through a homogeneous matrix-pore model.

Hydraulic fracturing is the primary stimulation method for shale oil reservoirs, but a considerable fraction of injected fracturing fluid may remain in the matrix–fracture system during the shut-in period. The retained fluid can interact with shale pores, bedding interfaces, clay minerals, and pre-existing microfractures. Therefore, shut-in imbibition should not be viewed only as a fluid-loss process; it is also a coupled oil-recovery and fluid–rock interaction process. Field and laboratory studies have shown that soaking or shut-in can influence well performance, water-blockage removal, fracturing-fluid retention, and hydrocarbon recovery in tight and shale reservoirs [10]. However, the effect of shut-in is not universally beneficial. Depending on pore connectivity, wettability, clay content, stress state, and fluid chemistry, imbibition may either promote oil displacement or aggravate liquid retention and formation damage [11]. Water adsorption and imbibition in shales may also induce microfracture development, salt diffusion, and stress redistribution [12]. These coupled effects are especially important in continental shale oil reservoirs, where the contribution of different pore-size domains to oil recovery remains difficult to quantify.

Spontaneous and forced imbibition are fundamentally controlled by capillary force, which depends on interfacial tension, wettability, and pore size. Classical capillary theory has long emphasized the roles of capillary pressure, boundary conditions, characteristic length, and wettability in controlling imbibition rate and recovery [13]. Later developments further clarified that spontaneous imbibition in porous media is affected by pore geometry, fluid properties, boundary conditions, and wetting state [14]. In shale and tight reservoirs, surfactants or imbibition agents are often added to fracturing fluids to reduce interfacial

tension, alter wettability, mitigate liquid blockage, and improve oil recovery. Alvarez and Schechter showed that surfactant additives can alter wettability and promote spontaneous imbibition in unconventional liquid reservoirs [15]. Sheng further discussed the importance of matching surfactant type with reservoir wettability and fluid properties when designing imbibition-enhanced oil recovery systems [16]. However, interfacial tension reduction alone does not necessarily guarantee improved recovery from all pore-size domains. Experimental studies have shown that interfacial tension reduction and wettability alteration may contribute differently to imbibition-enhanced oil recovery in low-permeability reservoirs [17]. Therefore, different imbibition agents may enhance recovery through distinct capillary-force regulation pathways, and their effects should be evaluated through coupled interfacial tension, apparent wettability, capillary pressure, and pore-size-dependent recovery.

Low-field nuclear magnetic resonance provides a powerful tool for tracking pore-scale fluid migration in tight rocks and shales. The transverse relaxation time T_2 is commonly related to pore size because short T_2 components are generally associated with fluids stored in small pores or nanopores, whereas long T_2 components correspond to larger pores, microfractures, or better-connected flow pathways [18]. NMR has become an important method for characterizing pore structure and fluid occurrence in unconventional reservoirs [19]. Time-lapse NMR has also been widely used to monitor imbibition-induced oil migration and remaining oil distribution in tight and shale reservoirs [20]. For example, NMR monitoring has revealed oil migration from nanometer-to-micrometer-sized pores during dynamic surfactant imbibition in tight rocks [21]. Recent NMR studies have further demonstrated that shale oil recovery during water imbibition involves a coupled nanopore-to-microfracture flow mechanism [22]. Compared with final recovery measurements, time-lapse NMR can resolve the dynamic contribution of different pore-size domains during imbibition, making it suitable for identifying whether nanopore-confined oil can be effectively mobilized during shut-in.

In addition to pore-size-resolved NMR analysis, fractal characterization provides an effective approach for quantifying the multiscale heterogeneity of shale pore systems. Fractal theory has been widely used to describe pore-size distribution, tortuosity, surface roughness, and permeability of porous media [23–25]. Fractal permeability models have shown that pore-size hierarchy and pore-network complexity can strongly influence fluid transport in porous media [24]. For shale reservoirs, pore fractal dimension has been used to quantify nanoscale pore complexity and to interpret permeability-related structural heterogeneity [25]. Pore-type-dependent fractal analysis has further shown that different shale pore types may contribute differently to pore complexity and permeability [23]. Integrated N_2 adsorption, mercury intrusion, and three-dimensional imaging have also been applied to characterize lacustrine shale pore structure and fractal features [24]. NMR- and SEM-derived fractal dimensions have recently been used to evaluate shale pore structure and multiscale heterogeneity [25]. These studies indicate that fractal dimension can provide a quantitative descriptor of pore-system complexity, but its relationship with shut-in imbibition recovery remains insufficiently understood.

Fractal analysis has also been extended from pore systems to fracture networks. CT-based reconstruction combined with box-counting methods has been used to quantify three-dimensional fracture-network geometry and fractal dimension in subsurface rocks [26]. Three-dimensional multifractal analysis has further demonstrated that fracture complexity in bedding shale can be quantitatively described using μ-CT imaging [27]. Fractal permeability models for rough fracture networks also show that fracture morphology, tortuosity, and spatial distribution strongly affect effective flow capacity [28]. These studies are highly relevant to shut-in imbibition because oil recovery and permeability en-

hancement in shale are often controlled by both nanopore accessibility and microfracture activation. However, few studies have linked NMR-derived fractal pore heterogeneity with capillary-force-regulated shut-in imbibition, pore-size-dependent recovery, apparent nanopore mobilization threshold, and post-imbibition permeability enhancement. This gap limits the mechanistic understanding of how retained fracturing fluid is converted into effective oil mobilization during the shut-in period.

In this study, LGS continental shale oil cores were used to investigate capillary-force-regulated pressurized shut-in imbibition. Two imbibition agents with different interfacial tension and wettability-regulation behaviors were selected to represent different capillary-force regulation pathways. Interfacial tension measurements, apparent contact angle tests, capillary pressure calculation, pressurized shut-in imbibition, time-lapse NMR monitoring, NMR-based fractal characterization, visual/CT observations, and permeability measurements before and after imbibition were integrated to establish a pore-size-dependent recovery and permeability-evolution framework. The objectives of this study are to: (1) quantify how the two imbibition agents regulate interfacial tension, apparent wettability, and capillary pressure; (2) evaluate total and pore-size-dependent recovery during pressurized shut-in imbibition; (3) derive NMR-based fractal dimensions to quantify the multiscale heterogeneity of the T_2-derived pore-size distribution; (4) identify the apparent mobilization threshold of nanopore-confined oil; (5) determine whether pressurized imbibition induces pore enlargement, microfracture activation, and permeability enhancement; and (6) provide implications for shut-in operation and imbibition-agent design in continental shale oil reservoirs.

2. Materials and Methods

2.1. Integrated Experimental Workflow

This study was designed as an integrated core-scale workflow to link capillary-force regulation, pore-size-dependent oil mobilization, and post-imbibition permeability evolution in LGS continental shale oil cores. The experiments were not conducted as isolated measurements on unrelated samples. Instead, the same core-scale research sequence was used to preserve the correspondence among initial petrophysical properties, interfacial behavior, pore–fracture structure, imbibition recovery, and post-imbibition permeability response. This workflow was adopted because shale oil recovery is strongly controlled by multiscale pore systems, nanopore connectivity, bedding-related heterogeneity, and fluid–rock interactions during shut-in. The integrated workflow consisted of six main steps. First, the basic petrophysical properties of the shale cores were measured, including core dimensions, porosity, and initial permeability. These measurements provided the baseline storage and flow capacity of each core. Second, oil–water interfacial tension and apparent contact angle were measured to quantify how the base fracturing fluid and two imbibition agents modified the oil–water and fluid–rock interfacial behavior. These data were further used to calculate capillary pressure in different pore-size domains, following the classical concept that capillary-driven imbibition is controlled by interfacial tension, wettability, and pore size. Third, CT scanning was conducted before imbibition to characterize the initial pore–fracture structure, bedding-related discontinuities, and visible microfractures. Fourth, the cores were saturated with crude oil and characterized by low-field NMR to obtain the initial oil distribution in different T_2-derived pore-size domains. Fifth, shut-in imbibition experiments were performed using fracturing fluids containing different imbibition agents. During imbibition, time-lapse NMR scanning was conducted at selected shut-in times to monitor oil-signal reduction and to calculate both total recovery and pore-size-dependent recovery. Finally, after imbibition, the cores were dried and retested for permeability. Post-imbibition CT scanning and visual observation were also performed to

identify pore enlargement, bedding-interface opening, or microfracture activation. This integrated workflow enabled the recovery behavior to be interpreted not only from final oil recovery, but also from the coupled evolution of interfacial properties, capillary pressure, pore-size-dependent oil mobilization, and pore–fracture structure. The integrated workflow consisted of six main steps, as illustrated in Figure 1.

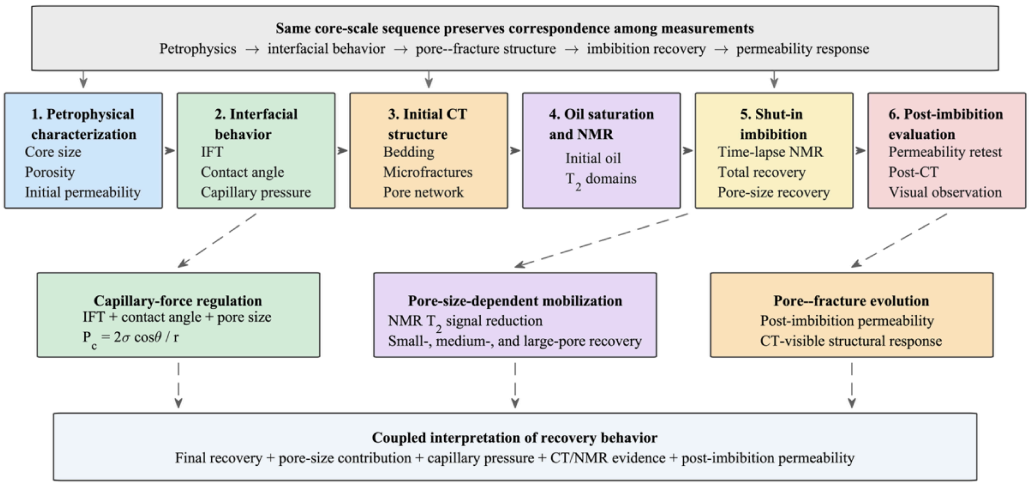


Figure 1. Integrated experimental workflow for evaluating capillary-force-regulated shut-in imbibition in LGS shale oil cores.

2.2. Shale Samples and Reservoir Background

The shale cores used in this study were collected from the LGS Formation, a lacustrine continental shale oil interval in China characterized by laminated fabrics, nanoscale pore-throat systems, and highly heterogeneous pore–fracture networks. Continental shale oil reservoirs commonly contain organic pores, inorganic nanopores, clay-related pores, intergranular pores, bedding-parallel discontinuities, and microfractures, which jointly control oil storage, movable oil saturation, and fluid transport. The selected LGS cores were therefore considered suitable for evaluating pore-size-dependent oil mobilization and permeability evolution during shut-in imbibition. Before imbibition, all cores were cleaned, dried, and characterized for basic petrophysical properties. Core dimensions, porosity, and initial gas permeability were measured to establish the baseline pore storage and flow capacity. Bedding orientation and visible microfracture features were recorded because bedding-related discontinuities and microfractures may strongly affect imbibition pathways, liquid retention, and post-imbibition permeability response. Bedding orientation and visible microfracture features were recorded to account for structural heterogeneity affecting imbibition pathways and permeability evolution. The experimental oil was obtained from the target shale oil reservoir or prepared to match the reservoir crude-oil properties. Mineralogical composition of representative samples was quantitatively characterized using X-ray diffraction (XRD), which confirms that the LGS shale is dominated by quartz (40.3–47.1%) and clay minerals (34.0–50.4%), with minor feldspar and carbonate content. The clay fraction is mainly composed of illite, illite/smectite mixed layers, and kaolinite, indicating strong surface reactivity and heterogeneous pore development. Oil density and viscosity were measured or recorded at the testing temperature because these properties affect oil mobility and NMR relaxation response. The basic core properties and experimental assignments are summarized in Table 1.

Table 1. Basic properties and experimental assignments of LGS shale cores used in this study.

Sample ID	Diameter (mm)	Length (mm)	Porosity (%)	Permeability (mD)	Imbibition Fluid
H-1#	25.47	50.06	0.4721	0.03983	Imbibition agent 1
H-2#	25.44	49.97	0.2756	0.01061	Imbibition agent 1
H-3#	25.49	50.32	0.7585	0.00351	Imbibition agent 1
H-4#	25.51	50.03	0.6281	0.03242	Imbibition agent 1
H-5#	25.43	49.89	0.1359	0.03875	Imbibition agent 2
H-6#	25.46	50	0.3713	0.08324	Imbibition agent 2
H-7#	25.53	50.13	1.0777	0.00360	Imbibition agent 2
H-8#	25.45	50.07	0.3355	0.02941	Imbibition agent 2

2.3. Imbibition Fluids and Capillary-Force Regulation Strategy

A base fracturing fluid and two imbibition-agent systems were used to investigate how interfacial tension reduction and wettability alteration regulate shut-in imbibition. The two imbibition agents were not treated simply as high- and low-performance additives. In this study, an imbibition agent is defined as a surfactant-based additive system that regulates oil–water interfacial tension and rock wettability, thereby modifying capillary-force-driven imbibition behavior in shale pore–fracture systems. Instead, they were selected to represent two different capillary-force regulation pathways involving different degrees of oil–water interfacial tension reduction and apparent wettability alteration. This design allowed the recovery response to be interpreted from the perspective of capillary-force redistribution rather than only from final oil recovery. Surfactants and imbibition agents have been widely used in shale and tight reservoirs to alter wettability, reduce interfacial tension, mitigate liquid blockage, and enhance oil recovery. However, previous studies have shown that interfacial tension reduction and wettability alteration may contribute differently to imbibition recovery, and that lowering interfacial tension alone does not necessarily guarantee higher recovery from all pore-size domains. Therefore, in this study, Agent 1 and Agent 2 were evaluated as two distinct capillary-force regulation systems. Four concentrations were considered for each imbibition-agent system: 0.05 wt%, 0.10 wt%, 0.15 wt%, and 0.20 wt%. Due to limited availability of homogeneous core samples, each concentration condition was tested on a single core sample. Therefore, no statistical replication (standard deviation or confidence interval) was performed. The base fracturing fluid without imbibition agent was used as the control fluid. All fluids were prepared using the same base water and mixed until visually homogeneous before the interfacial tension, contact angle, and shut-in imbibition tests. The composition and tested concentrations of the imbibition fluids are summarized in Table 2. This design is consistent with previous findings that interfacial tension reduction and wettability alteration may contribute differently to imbibition-enhanced recovery [17].

The two imbibition agents used in this study are commercial surfactant-based oilfield chemical systems supplied for hydraulic fracturing and enhanced oil recovery operations in unconventional reservoirs. The trade names and detailed formulations are proprietary and therefore not disclosed; however, their classification is provided at the industrial application level to ensure material traceability while respecting supplier confidentiality. Importantly, the functional characteristics of the two agents are distinguished based on experimentally measured interfacial properties rather than compositional information. Specifically, Agent 1 is defined as a wettability-modifying surfactant-dominant system, whereas Agent 2 is defined as a system characterized by stronger interfacial tension-reduction capability with

auxiliary co-surfactant components. Therefore, their roles in this study are defined in terms of capillary-force regulation pathways rather than detailed chemical formulations.

Table 2. Composition and tested concentrations of imbibition fluids (base fluid: Formation-compatible water + Friction reducer + clay stabilizer + cleanup additive).

Sample ID	Fluid Code	Base Additive Package	Imbibition Agent	Concentration (wt%)
H-1#	A1-0.05	Same as base fluid	Agent 1	0.05
H-2#	A1-0.10	Same as base fluid	Agent 1	0.1
H-3#	A1-0.15	Same as base fluid	Agent 1	0.15
H-4#	A1-0.20	Same as base fluid	Agent 1	0.2
H-5#	A2-0.05	Same as base fluid	Agent 2	0.05
H-6#	A2-0.10	Same as base fluid	Agent 2	0.1
H-7#	A2-0.15	Same as base fluid	Agent 2	0.15
H-8#	A2-0.20	Same as base fluid	Agent 2	0.2

The distinct behaviors of Agent 1 and Agent 2 can be further interpreted from an interfacial partitioning perspective. Surfactant molecules in Agent 1 tend to preferentially interact with the rock surface, leading to stronger wettability modification, whereas Agent 2 exhibits a higher tendency to accumulate at the oil–water interface, resulting in more pronounced interfacial tension reduction. This difference in interfacial affinity provides a physical basis for the observed dual capillary-force regulation pathways.

Although the exact chemical formulations of the two imbibition agents are proprietary, their functional performance is fully characterized in this study through measurable interfacial parameters, including oil–water interfacial tension, apparent contact angle, and the combined capillary term $\sigma\cos\theta$. These parameters define a reproducible physicochemical framework for capillary-force regulation. Accordingly, equivalent capillary-force conditions can be reproduced by matching interfacial tension, apparent contact angle, and capillary-force characteristics using alternative surfactant systems with similar interfacial responses.

2.4. Interfacial Tension and Apparent Contact Angle Measurements

2.4.1. Interfacial Tension Measurement

Oil–water interfacial tension was measured to quantify the effect of the imbibition agents on the fluid–fluid interface. The experimental oil and each imbibition fluid were equilibrated at the target testing temperature before measurement. Interfacial tension was measured using a standard interfacial tension instrument. Each fluid system was tested repeatedly, and the average value was used in the capillary pressure calculation. Measurement uncertainty was evaluated using repeated measurements. The interfacial tension data were used to determine whether each imbibition agent mainly reduced the oil–water interfacial barrier or reached an interfacial tension plateau at a given concentration. This distinction is important because interfacial tension reduction affects capillary entry resistance and displacement behavior, but the relationship between interfacial tension and oil recovery can be nonlinear in tight and shale reservoirs. In nanopore-dominated systems, oil mobilization is also affected by pore accessibility, oil adsorption, wettability, and pore-throat connectivity.

2.4.2. Apparent Contact Angle Measurement

Apparent contact angle was measured to evaluate the wettability-regulation effect of the imbibition fluids on LGS shale surfaces. Because shale surfaces are rough, laminated,

and compositionally heterogeneous, the measured contact angle was treated as an apparent contact angle rather than an intrinsic mineral-scale contact angle. This treatment is consistent with the understanding that shale wettability is affected by mineral composition, organic matter, surface roughness, pore structure, and local heterogeneity. Fresh or polished shale slices were first oil-aged under controlled conditions. Droplets of the corresponding imbibition fluid were then placed on the oil-aged shale surface, and images were recorded after the droplet reached a stable morphology. The apparent contact angle was calculated using image-analysis software. Each condition was measured at multiple locations to account for heterogeneity caused by bedding, mineral distribution, and microfractures. The average apparent contact angle was used together with interfacial tension to calculate capillary pressure in different pore-size domains.Oil–water interfacial tension was measured to quantify the effect of the imbibition agents on the fluid–fluid interface (Figure 2a) Apparent contact angle was measured to evaluate the wettability-regulation effect of the imbibition fluids on LGS shale surfaces (Figure 2b).The resulting capillary-force parameter (σcosθ) is shown in Figure 2c.

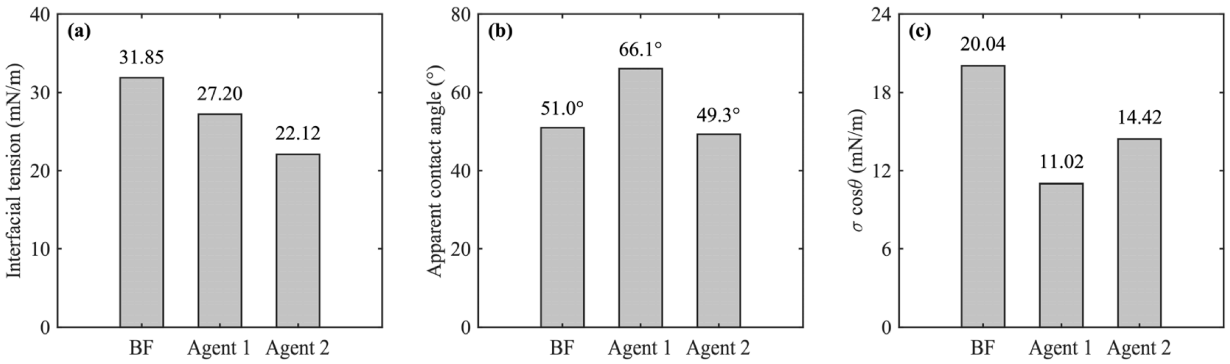


Figure 2. Comparison of capillary-force-related parameters for the base fluid (BF), Agent 1, and Agent 2. (**a**) Oil–water interfacial tension; (**b**) apparent contact angle; and (**c**) capillary-force indicator (σcosθ).

2.5. Capillary Pressure Calculation in Different Pore-Size Domains

Capillary pressure was calculated to link interfacial behavior with pore-size-dependent imbibition. For a simplified cylindrical pore, the capillary pressure can be expressed as:

$$P_c = \frac{2\sigma\cos\theta}{r} \quad (1)$$

where P_c is capillary pressure, σ is oil–water interfacial tension, θ is apparent contact angle, and r is pore radius.

Although shale pore systems are not ideal cylindrical capillaries, Equation (1) provides a first-order framework for comparing how different imbibition fluids modify the capillary-force distribution in different pore-size domains. The pore-size domains were divided according to the NMR-derived pore-size interpretation and the pore-throat characteristics of shale oil reservoirs. In this study, the pore-size domains were classified as 0–5 nm, 5–10 nm, 10–20 nm, and >20 nm. The 0–5 nm and 5–10 nm intervals represent nanopore-dominated storage spaces, the 10–20 nm interval represents small pore throats or transition pores, and the >20 nm interval represents relatively large pores, bedding-related pores, and microfracture-associated storage and flow spaces (Figure 3). For each imbibition fluid, capillary pressure was calculated using the measured interfacial tension and apparent contact angle. The calculated curves were compared to identify how Agent 1 and Agent 2 changed the capillary driving force or capillary entry resistance across different pore sizes.

Similar capillary concepts have been widely used to interpret spontaneous imbibition and wettability-controlled fluid displacement in porous media [13,14]. The calculation was not used to assign an exact pore-scale pressure in each irregular shale pore; instead, it was used to compare the relative capillary-force regulation ability of different fluids.

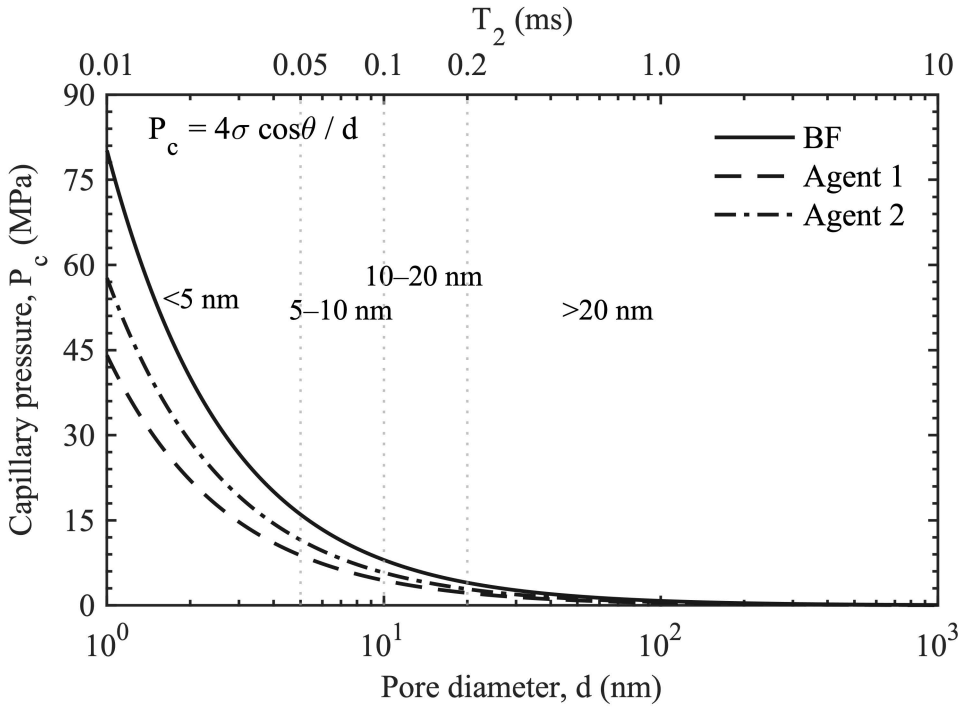


Figure 3. Calculated capillary pressure as a function of pore diameter for different imbibition fluids. The upper *x*-axis shows the corresponding T_2 values. The vertical dotted lines divide the pore-diameter intervals of <5 nm, 5–10 nm, 10–20 nm, and >20 nm.

2.6. Initial CT Characterization, Oil Saturation, and NMR Measurement

Before shut-in imbibition, CT scanning was performed on selected dry shale cores to characterize the initial pore–fracture structure. The CT images were used to document bedding-related discontinuities, visible microfractures, and larger pore–fracture features. CT images were used for qualitative structural observation because the samples had already experienced imbibition-induced structural disturbance, limiting strict quantitative fracture segmentation. The initial CT data provided a structural baseline for identifying post-imbibition pore enlargement or microfracture activation. The initial CT data provided a structural baseline for identifying post-imbibition pore enlargement or microfracture activation. Because shale pore systems extend from nanometer-scale pores to micrometer-scale fractures, CT mainly captured relatively large pores and fractures, whereas NMR was used to evaluate fluid distribution over different pore-size domains. After initial CT scanning and petrophysical testing, the cores were dried to remove residual water and volatile components. The drying temperature and duration were selected to avoid thermal alteration of clay minerals and organic matter. After drying, the cores were weighed and evacuated in a vacuum chamber. Crude oil was then introduced under vacuum, followed by pressure-assisted saturation to improve oil filling in nanopores and microfractures. The oil-saturated cores were aged under controlled temperature and pressure to establish oil–rock interaction before NMR measurement. Low-field NMR was used to characterize the initial oil distribution and to monitor time-dependent oil mobilization during imbibition. The transverse relaxation time distribution was obtained using a Carr–Purcell–Meiboom–Gill pulse sequence. NMR was widely applied to characterize pore structure, fluid distribution,

and imbibition-induced oil migration in tight and shale reservoirs [18,19]. In general, short T_2 components correspond to fluids stored in small pores or nanopores, whereas long T_2 components are associated with larger pores, microfractures, or less restricted fluid spaces. The relationship between T_2 and pore size can be expressed as:

$$\frac{1}{T_2} = \rho_2 \frac{S}{V} \tag{2}$$

where ρ_2 is surface relaxivity, and S/V is the pore surface-to-volume ratio. For a simplified cylindrical pore, this relationship can be converted to:

$$r = CT_2 \tag{3}$$

where r is the equivalent pore radius and C is the pore-size conversion coefficient.

If mercury-intrusion capillary pressure, nitrogen adsorption, or other pore-size calibration data are available, C should be obtained by matching the cumulative pore-size distribution with the cumulative NMR signal. If direct calibration is unavailable, the T_2-derived pore-size domains are used to compare relative oil mobilization among different pore-size ranges rather than to define absolute pore sizes. The initial NMR T_2 distributions of the oil-saturated LGS shale cores, which served as the basis for the subsequent poresize-domain analysis, are shown in Figure 4.

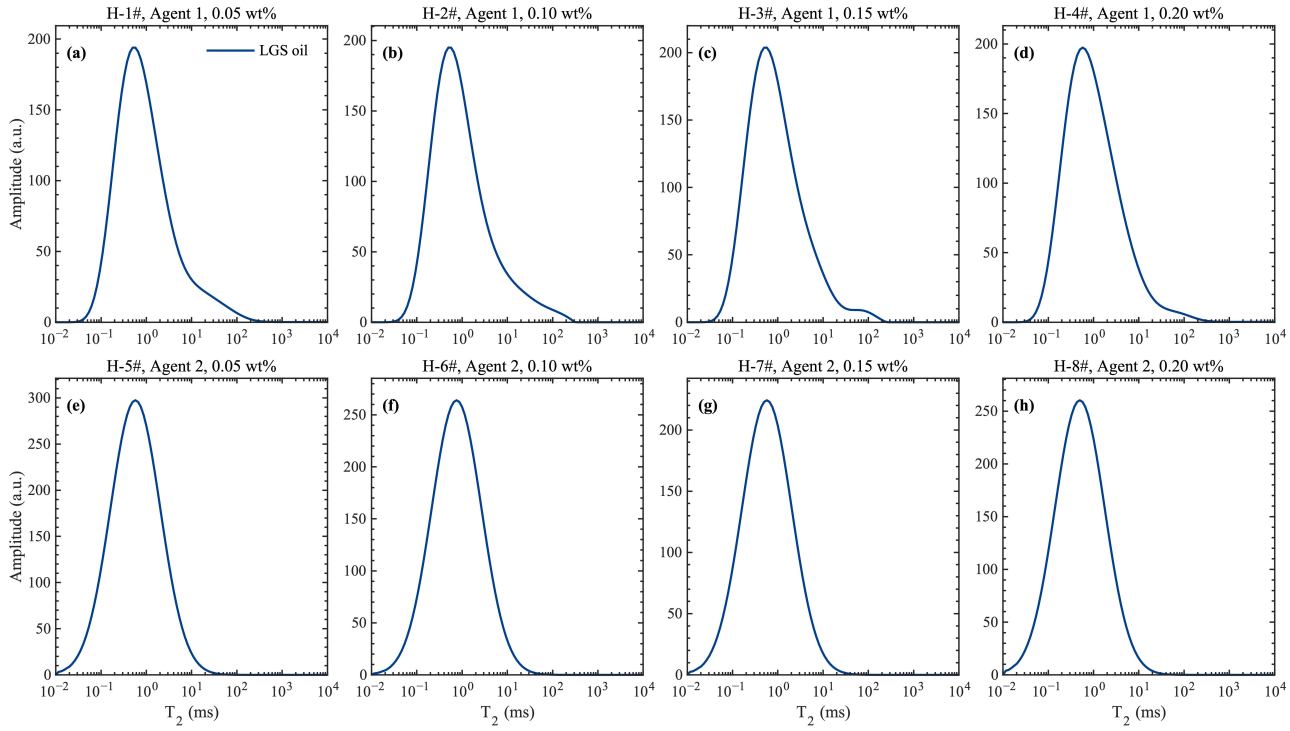


Figure 4. Initial NMR characterization of oil-saturated LGS shale cores. (**a**) H-1#, Agent 1, 0.05 wt%; (**b**) H-2#, Agent 1, 0.10 wt%; (**c**) H-3#, Agent 1, 0.15 wt%; (**d**) H-4#, Agent 1, 0.20 wt%; (**e**) H-5#, Agent 2, 0.05 wt%; (**f**) H-6#, Agent 2, 0.10 wt%; (**g**) H-7#, Agent 2, 0.15 wt%; (**h**) H-8#, Agent 2, 0.20 wt%.

2.7. Shut-In Imbibition and Time-Lapse NMR Monitoring

Shut-in imbibition experiments were conducted to simulate the post-fracturing contact between retained fracturing fluid and oil-saturated shale matrix. After oil saturation and initial NMR measurement, each core was placed in an imbibition cell containing the corresponding imbibition fluid. The cell was maintained under the target experimental temperature and pressure conditions designed to represent the shut-in environment of

the target reservoir. This design allowed the imbibition fluid to contact the oil-saturated shale core under controlled conditions rather than as an uncontrolled ambient exposure. During the shut-in experiment, the cores were removed at selected time intervals for NMR measurement and then returned to the imbibition cell to continue the test. The measurement time points were 1, 6, 12, 24, 48, 72, 96, 120, and 144 h. The corresponding time-lapse NMR T_2 distributions obtained during the shut-in imbibition process are shown in Figure 5. These time points were selected to capture the early rapid recovery stage, the intermediate slow imbibition stage, and the late plateau or structural-response stage. Before each NMR measurement, the core surface was gently wiped to remove external fluid without disturbing fluids inside the pore system. The shut-in design was used to better represent fluid invasion, oil displacement, and fluid–rock interaction during the post-fracturing shut-in period, which may not be fully captured by conventional atmospheric static imbibition tests.

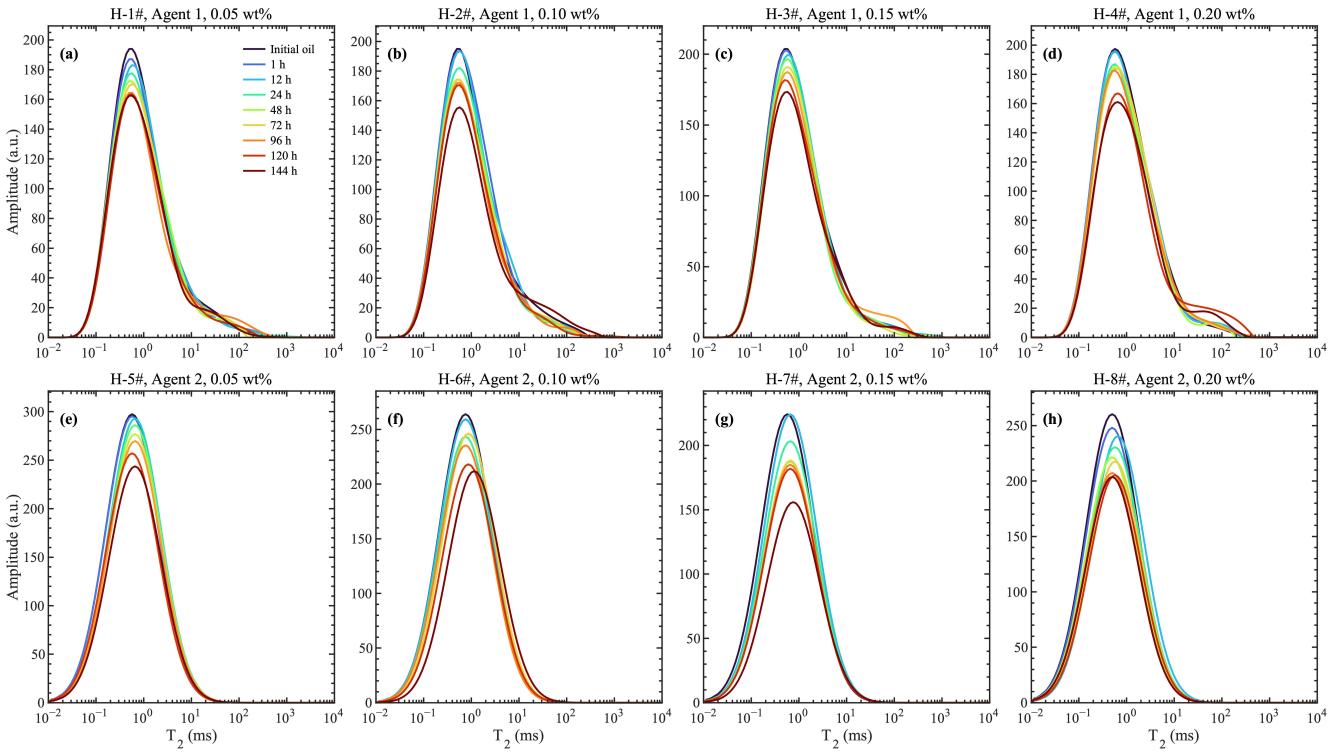


Figure 5. Time-lapse NMR T_2 distributions of oil-saturated LGS shale cores during shut-in imbibition under different imbibition-agent systems and concentrations. (**a**) H-1#, Agent 1, 0.05 wt%; (**b**) H-2#, Agent 1, 0.10 wt%; (**c**) H-3#, Agent 1, 0.15 wt%; (**d**) H-4#, Agent 1, 0.20 wt%; (**e**) H-5#, Agent 2, 0.05 wt%; (**f**) H-6#, Agent 2, 0.10 wt%; (**g**) H-7#, Agent 2, 0.15 wt%; (**h**) H-8#, Agent 2, 0.20 wt%.

2.8. Calculation of Total and Pore-Size-Dependent Recovery

The total oil recovery during shut-in imbibition was calculated from the decrease in NMR signal amplitude. The total recovery at time t was defined as:

$$R(t) = \frac{S_0 - S_t}{S_0} \times 100\% \quad (4)$$

where S_0 is the initial total NMR signal of the oil-saturated core, and S_t is the total NMR signal after imbibition for time t. The decrease in NMR signal was interpreted as oil mobilized from the core during imbibition.

To evaluate pore-size-dependent oil recovery, the NMR signal was integrated over each pore-size domain. The contribution of pore-size domain i to total recovery was calculated as:

$$R_i(t) = \frac{S_{i,0} - S_{i,t}}{S_0} \times 100\% \quad (5)$$

where $S_{i,0}$ and $S_{i,t}$ are the NMR signals of pore-size domain i before imbibition and after imbibition for time t, respectively. This parameter quantifies how much each pore-size domain contributes to total recovery.

The internal mobilization degree of pore-size domain i was further calculated as:

$$M_i(t) = \frac{S_{i,0} - S_{i,t}}{S_{i,0}} \times 100\% \quad (6)$$

where $M_i(t)$ represents the fraction of oil mobilized from a specific pore-size domain. Using both $R_i(t)$ and $M_i(t)$ avoids ambiguity between contribution to total recovery and mobilization efficiency within a given pore-size range. This distinction is important for identifying whether a small pore-size domain contributes little because it contains limited initial oil or because the oil in that domain is difficult to mobilize.

2.9. NMR-Based Fractal Characterization of Pore-Size Distribution

To further quantify the multiscale heterogeneity of the LGS shale pore system, an NMR-based fractal characterization method was introduced based on the T_2-derived pore-size distribution. Shale reservoirs commonly contain nanopores, transition pores, larger pores, bedding-related voids, and microfracture-associated storage spaces. Such pore systems are highly heterogeneous and often exhibit scale-dependent or fractal characteristics. Therefore, the fractal dimension derived from the NMR T_2 spectrum can provide a quantitative descriptor of pore-size complexity and can be used to interpret pore-size-dependent oil mobilization during shut-in imbibition. NMR-derived and image-based fractal dimensions have been widely used to describe shale pore heterogeneity and fracture-network complexity [25,26].

The NMR T_2 spectrum was first converted into an equivalent pore-size distribution using the pore-size conversion relationship described in Equation (3). Because the same conversion coefficient was applied to all samples, the calculated fractal parameters were used mainly for relative comparison among cores and imbibition fluids rather than for defining absolute pore sizes. The cumulative NMR signal was then calculated from the T_2-derived pore-size distribution. For a fractal pore system, the cumulative pore volume and pore radius can be related by a power-law relationship:

$$\frac{S_{\text{cum}}(r)}{S_{\text{total}}} = \left(\frac{r}{r_{\text{max}}}\right)^{3-D_f} \quad (7)$$

where $S_{\text{cum}}(r)$ is the cumulative NMR signal corresponding to pores with radius smaller than r, S_{total} is the total NMR signal, r is the equivalent pore radius converted from T_2, r_{max} is the maximum equivalent pore radius considered in the fitting interval, and D_f is the NMR-derived pore fractal dimension. Taking the logarithm of both sides gives:

$$\log\left[\frac{S_{\text{cum}}(r)}{S_{\text{total}}}\right] = \left(3 - D_f\right)\log\left(\frac{r}{r_{\text{max}}}\right) \quad (8)$$

Thus, the slope K of the log–log relationship between $S_{\text{cum}}(r)/S_{\text{total}}$ and r/r_{max} can be obtained by linear regression:

$$K = 3 - D_f \quad (9)$$

and the fractal dimension can be calculated as:

$$D_f = 3 - K \tag{10}$$

In this study, the fitting was performed over the effective T_2-derived pore-size interval where the NMR signal was above the noise level and the cumulative signal showed an approximately linear relationship in log–log coordinates. Very low-amplitude endpoints were excluded to avoid unstable fitting caused by instrumental noise, signal truncation, or isolated long-T_2 components. The coefficient of determination, R^2, was used to evaluate the reliability of the fractal fitting. A larger D_f indicates a more complex and heterogeneous pore-size distribution, whereas a smaller D_f indicates a relatively simpler pore system with weaker multiscale heterogeneity.

To link fractal pore structure with shut-in imbibition behavior, the initial fractal dimension $D_{f,0}$ was calculated from the NMR spectrum of each oil-saturated core before imbibition. Where appropriate, the post-imbibition fractal dimension $D_{f,t}$ was also calculated from the NMR spectrum after a given shut-in time to evaluate whether imbibition caused measurable changes in pore-size distribution. The fractal dimension variation was expressed as:

$$\Delta D_f = D_{f,t} - D_{f,0} \tag{11}$$

A positive ΔD_f suggests increased pore-size heterogeneity or enhanced contribution from newly activated pore–fracture spaces, whereas a negative or negligible ΔD_f indicates limited structural modification or preferential removal of oil from certain pore-size domains. In addition, the relationship between D_f, total recovery, pore-size-dependent recovery contribution, nanopore mobilization threshold, and permeability enhancement was examined to clarify how fractal pore heterogeneity controls capillary-force-regulated shut-in imbibition.

It should be noted that the NMR-derived fractal dimension represents an effective pore-size-distribution descriptor rather than a direct three-dimensional geometric fractal dimension. The calculated D_f is influenced by pore-size distribution, fluid occurrence state, surface relaxation, pore connectivity, and the selected fitting interval. Therefore, it was used in this study as a comparative indicator of multiscale pore heterogeneity and imbibition accessibility under the same experimental and data-processing framework.

2.10. Post-Imbibition Permeability and CT Characterization

After the shut-in imbibition experiments, selected cores were subjected to permeability testing, CT imaging, and visual observation to evaluate whether imbibition induced pore enlargement, microfracture activation, or permeability enhancement. The post-imbibition cores were first dried under controlled conditions and then retested for gas permeability. Dry-core permeability was used to reduce the influence of residual liquid saturation and to determine whether the permeability change reflected structural modification rather than a temporary fluid-blocking effect. The permeability enhancement ratio was calculated as:

$$E_k = \frac{k_{\text{after}} - k_{\text{before}}}{k_{\text{before}}} \times 100\% \tag{12}$$

where k_{before} and k_{after} are the dry-core permeability before and after shut-in imbibition, respectively. When $E_k > 0$, the core was classified as showing permeability enhancement.

For cores showing permeability reduction, the permeability damage ratio was calculated as:

$$D_k = \frac{k_{\text{before}} - k_{\text{after}}}{k_{\text{before}}} \times 100\% \tag{13}$$

where $D_k > 0$ indicates permeability impairment. Permeability enhancement was interpreted as evidence of improved connected flow pathways, potentially caused by pore enlargement, bedding-interface opening, or microfracture activation. Permeability impairment was interpreted as possible evidence of liquid retention, clay interaction, particle migration, or pore-throat blockage.

Post-imbibition CT scanning was performed to compare visible pore–fracture features before and after imbibition. Core photographs were also used to document surface fractures, bedding separation, or macroscopic structural changes. In addition, the NMR spectra before and after imbibition were compared to identify whether the T_2 distribution shifted toward longer relaxation times. An increase in long-T_2 signal or a rightward shift in the T_2 distribution was used to evaluate enhanced large-pore or microfracture-related storage space, provided that the change was consistent with CT, visual, and permeability data. Similar multi-evidence interpretation is necessary because NMR signal changes alone may be affected by fluid type, saturation, and surface relaxation.

3. Results

3.1. Interfacial Tension Reduction and Wettability Alteration

The two imbibition agents exhibited distinct interfacial-regulation behaviors, as reflected by the measured oil–water interfacial tension, apparent contact angle, and the combined term $\sigma\cos\theta$ (Figure 2). The base fracturing fluid showed an interfacial tension of 31.85 mN/m and an apparent contact angle of 51.0° on the oil-aged LGS shale surface. After adding Agent 1, the interfacial tension decreased to 27.20 mN/m, while the apparent contact angle increased to 66.1°. Agent 2 further reduced the interfacial tension to 22.12 mN/m, whereas the apparent contact angle decreased slightly to 49.3°. These results indicate that Agent 1 and Agent 2 regulated capillary force through different pathways. Agent 1 produced a moderate reduction in interfacial tension but caused a pronounced change in apparent wettability. The increase in apparent contact angle reduced the value of $\cos\theta$, thereby decreasing the effective capillary-force term despite the reduction in interfacial tension. In contrast, Agent 2 produced the lowest interfacial tension while maintaining a relatively favorable apparent contact angle. As a result, the calculated $\sigma\cos\theta$ decreased from 20.04 mN/m for the base fluid to 11.02 mN/m for Agent 1 and 14.42 mN/m for Agent 2. The interfacial measurements show that the two agents should not be evaluated only by interfacial tension or only by contact angle. Agent 1 is mainly characterized by apparent wettability alteration, whereas Agent 2 is characterized by stronger interfacial tension reduction with a more favorable combined capillary-force response. Therefore, the concentration-dependent recovery behavior needs to be interpreted through the coupled effect of σ, θ, and pore size rather than through a single interfacial parameter.

3.2. Capillary Pressure Response in Different Pore-Size Domains

The calculated capillary pressure curves show a strong dependence on pore diameter (Figure 3). For all fluid systems, capillary pressure increased sharply as pore diameter decreased from the large-pore range to the nanopore range. This trend follows the capillary pressure relationship. Therefore, the capillary pressure response is most sensitive in the smallest pore-size domains. The base fluid produced the highest capillary pressure over the full pore-size range, followed by Agent 2 and then Agent 1. In the <5 nm domain, the calculated capillary pressure remained high for all fluids, indicating strong capillary confinement and a high sensitivity to changes in interfacial properties. In the 5–10 nm and 10–20 nm domains, the capillary pressure decreased rapidly with increasing pore diameter, but the difference among the three fluids remained visible. In the >20 nm domain, the calculated capillary pressure became much lower, indicating that fluid exchange and oil

mobilization are more likely to occur in larger pores and microfracture-related spaces. The comparison between Agent 1 and Agent 2 confirms that interfacial tension reduction alone cannot fully describe imbibition behavior. Although Agent 2 had the lowest interfacial tension, Agent 1 showed the lowest calculated capillary pressure curve because of its larger apparent contact angle and smaller $\sigma\cos\theta$. Therefore, capillary-force regulation in LGS shale should be understood as a coupled response of interfacial tension, apparent wettability, and pore diameter. These results also suggest that the smallest nanopores may not be effectively mobilized simply by changing interfacial properties. Although capillary pressure is high in the <5 nm and 5–10 nm domains, actual oil recovery from these pores can still be restricted by oil adsorption, poor pore-throat connectivity, and limited accessibility of imbibition-agent molecules. Thus, the calculated capillary pressure response provides the physical basis for interpreting the subsequent pore-size-dependent recovery, but it should not be directly equated with recoverable oil from all nanopores.

3.3. Time-Dependent Total Recovery During Pressurized Shut-In Imbibition

The total oil recovery calculated from NMR signal reduction increased with shut-in time for all LGS shale cores, but the recovery trajectories differed markedly among samples and imbibition-agent concentrations (Figure 6). The final total recovery after 144 h ranged from approximately 12% to more than 30%, indicating that shut-in imbibition can mobilize a measurable fraction of oil from the LGS shale cores, but the efficiency is strongly sample- and fluid-dependent. For the Agent 1 system, total recovery increased continuously with time, but the final recovery varied with concentration. H-2# treated with A1-0.10 reached the highest final recovery among the Agent 1 samples, approximately 16%. H-1#, H-3#, and H-4# showed final recoveries of about 12–14%. The A1-0.05 sample showed gradual recovery growth, whereas A1-0.10 showed an early increase followed by continued late-stage recovery. A1-0.20 displayed stronger fluctuation during the middle stage, suggesting that recovery was affected by heterogeneous pore–fracture connectivity rather than by concentration alone. For the Agent 2 system, the recovery response was generally stronger than that of Agent 1. H-7# treated with A2-0.15 showed the highest recovery value among the tested samples, reaching approximately 30% at 144 h. H-8# treated with A2-0.20 also showed high recovery, exceeding 20%, and H-6# treated with A2-0.10 reached nearly 20%. H-5# treated with A2-0.05 showed a lower but still continuous increase, reaching approximately 18% at the end of the test. These results indicate that Agent 2 generally exhibited a stronger imbibition trend compared with Agent 1 under the tested conditions. The time-dependent curves can be divided into three stages. Stage I occurred during the first 24 h, during which many samples showed a rapid increase in total recovery. This early recovery is mainly attributed to oil mobilization from larger pores, connected pore throats, and microfracture-related spaces. Stage II occurred from approximately 24 to 96 h, when the recovery rate generally decreased or fluctuated, indicating that oil mobilization shifted toward less accessible pore spaces. Stage III occurred from 96 to 144 h, during which some samples approached a plateau, whereas others continued to increase. The continued late-stage recovery in H-6#, H-7#, and H-8# suggests that imbibition may have progressively accessed additional connected pore–fracture pathways.

Overall, the total recovery results show that Agent 2 achieved higher recovery than Agent 1 under comparable concentration ranges, with the strongest response observed at A2-0.15 (Figure 7). However, the non-monotonic concentration dependence suggests that the recovery behavior may be influenced by both fluid formulation and initial pore–fracture structure.

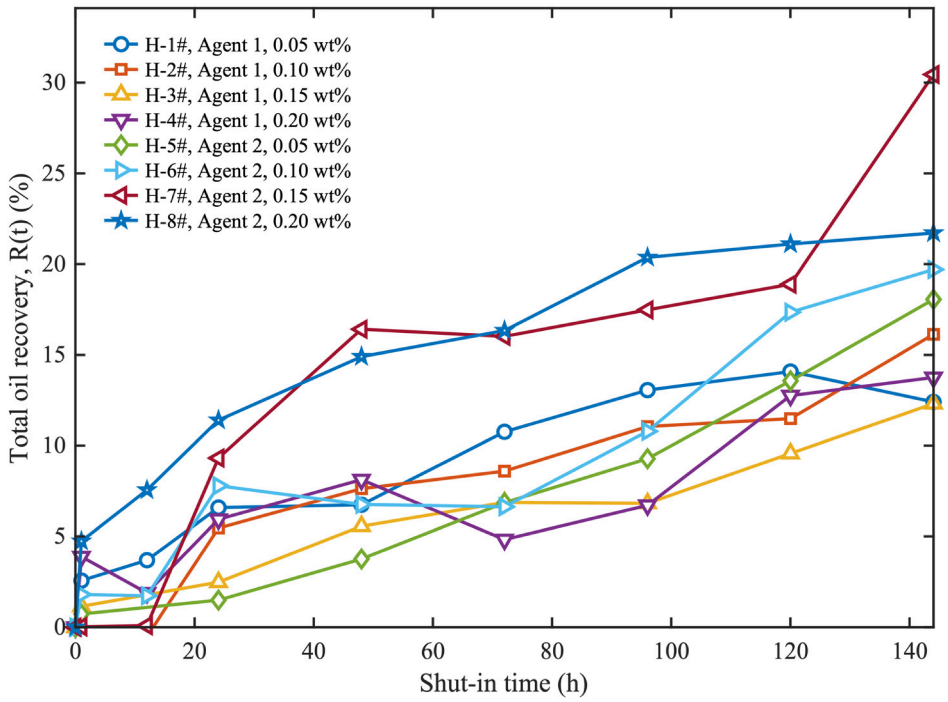


Figure 6. Time-dependent total oil recovery of LGS shale cores during shut-in imbibition calculated from NMR signal reduction.

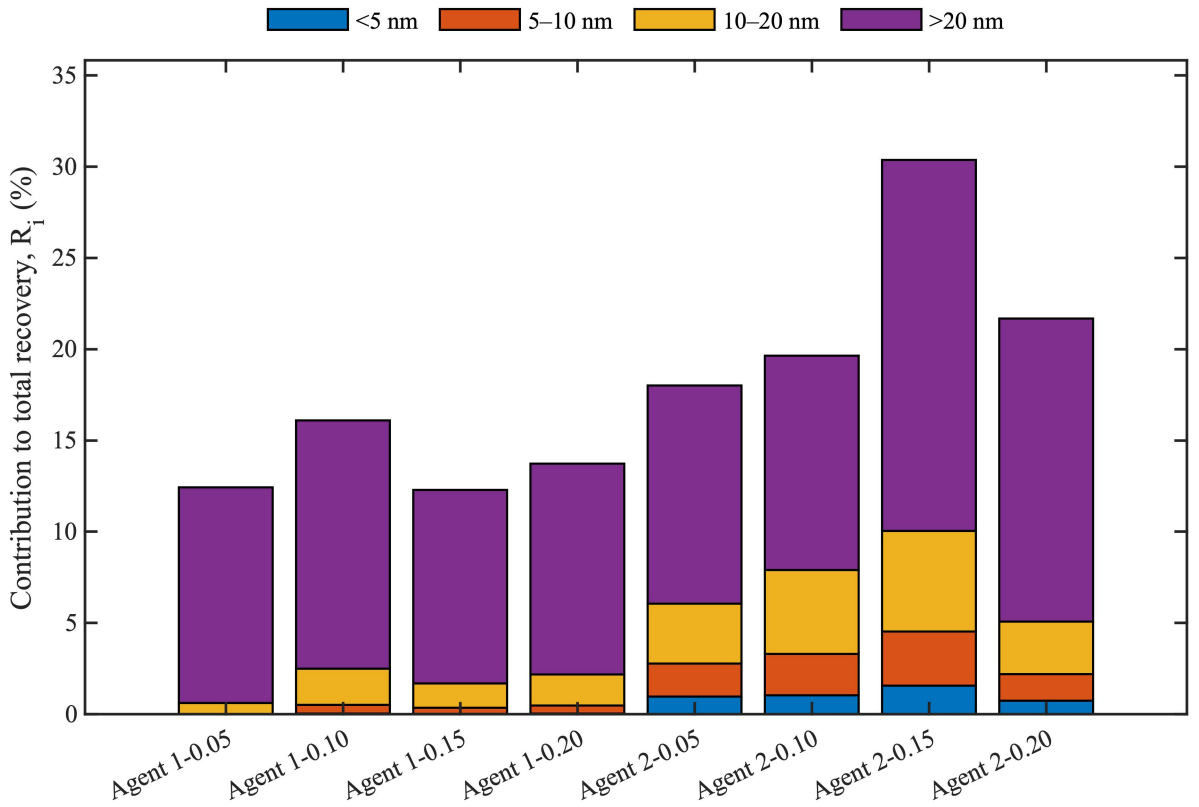


Figure 7. Time-lapse NMR T_2 spectra during shut-in imbibition.

3.4. NMR-Derived Fractal Characteristics and Concentration-Dependent Imbibition Response

The NMR-derived fractal dimension was calculated to quantify the multiscale heterogeneity of the T_2-derived pore-size distribution in the LGS shale oil cores. The concentration-dependent fractal and imbibition responses of Agent 1 and Agent 2 are shown in Figure 8.

Overall, the initial fractal dimension $D_{f,0}$ ranged from approximately 2.32 to 2.61, indicating that the LGS shale oil cores contained a heterogeneous multiscale pore system rather than a uniform capillary-bundle-type pore structure. This result is consistent with the coexistence of nanopores, transition pores, larger pores, bedding-related voids, and microfracture-associated storage spaces in continental shale oil reservoirs. The relatively small variation in fractal dimension suggests that the NMR-derived D_f is more sensitive to pore-size distribution than to connectivity reconstruction, indicating that shut-in imbibition primarily modifies flow-accessible pathways rather than the global pore topology.

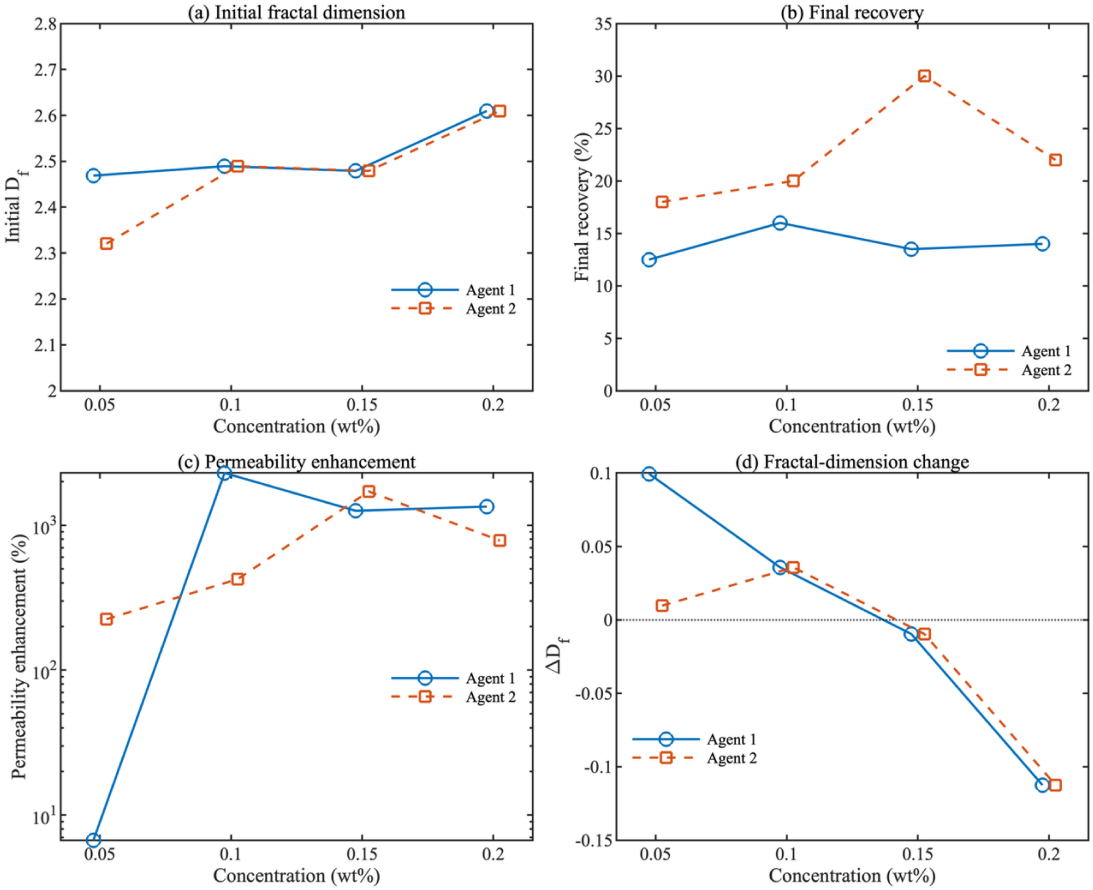


Figure 8. Concentration-dependent NMR-derived fractal characteristics, oil recovery, and permeability enhancement of LGS shale oil cores treated with Agent 1 and Agent 2. (**a**) Initial fractal dimension as a function of imbibition-agent concentration. (**b**) Final oil recovery after 144 h of shut-in imbibition. (**c**) Post-imbibition permeability enhancement. (**d**) Change in fractal dimension before and after imbibition. Agent 2 showed a more pronounced concentration-dependent recovery trend than Agent 1, with the optimum performance at 0.15 wt%. The small variation in D_f indicates that shut-in imbibition mainly activated accessible pore–fracture pathways rather than uniformly reconstructing the global pore-size distribution. The variation in fractal dimension is further interpreted within the context of a clay-rich, quartz-dominated mineral framework revealed by XRD analysis.

The two imbibition agents produced different interfacial and wettability-regulation characteristics, which provide the basis for interpreting their different concentration responses. The base fracturing fluid had an oil–water interfacial tension of 31.85 mN/m and an apparent contact angle of 51.0° on the oil-aged LGS shale surface. After adding Agent 1, the interfacial tension decreased moderately to 27.20 mN/m, whereas the apparent contact angle increased to 66.1°. This suggests that Agent 1 may mainly regulate imbibition through apparent wettability alteration. However, the increase in apparent contact angle reduced cosθ, causing the effective capillary-force term σcosθ to decrease to 11.02 mN/m.

In contrast, Agent 2 reduced the interfacial tension more strongly to 22.12 mN/m while maintaining a favorable apparent contact angle of 49.3°, resulting in a σcosθ value of 14.42 mN/m. Therefore, Agent 2 provided a different regulation pathway by reducing the oil–water interfacial barrier while preserving a more favorable apparent wettability condition for imbibition into connected pore–fracture domains.

For the Agent 1 system, the initial fractal dimension varied only slightly with concentration, remaining mainly between approximately 2.47 and 2.61 (Figure 8a). The final fractal dimension after shut-in imbibition was also close to the initial value, although the direction of ΔD_f changed with concentration. At 0.05 wt% and 0.10 wt%, ΔD_f was positive, whereas at 0.15 wt% and 0.20 wt%, ΔD_f became slightly negative. This indicates that Agent 1 caused limited changes in the global pore-size-distribution heterogeneity. The final recovery of Agent 1 increased from 12.5% at 0.05 wt% to 16.0% at 0.10 wt%, and then remained at a relatively low level of 13.5–14.0% at higher concentrations (Figure 8b). Although Agent 1 modified the apparent wettability of the oil-aged shale surface, the increased contact angle and reduced $\sigma\cos\theta$ did not lead to a continuous improvement in oil recovery. This suggests that apparent wettability alteration alone was insufficient to overcome the accessibility limitation of oil stored in the fractal nanopore–microfracture system of LGS shale.

The permeability enhancement of Agent 1 showed a stronger non-monotonic response. A slight permeability increase was observed at 0.05 wt%, whereas much larger enhancement occurred at 0.10–0.20 wt% (Figure 8c). Therefore, for Agent 1, the best recovery response occurred at 0.10 wt%, but the permeability enhancement did not strictly follow the recovery trend. This indicates that the permeability increase was more closely related to local pore-throat enlargement, bedding-interface opening, or microfracture activation than to a substantial increase in bulk oil recovery.

For the Agent 2 system, the initial fractal dimension increased from approximately 2.32 at 0.05 wt% to approximately 2.61 at 0.20 wt% (Figure 8a), reflecting differences in the initial pore-size heterogeneity among the selected cores. However, the final fractal dimension remained close to the initial value for most samples, and ΔD_f was small except at 0.20 wt%, where a more obvious negative change was observed (Figure 8d). The final recovery of Agent 2 showed a clearer concentration-dependent pattern than Agent 1. Recovery increased from 18.0% at 0.05 wt% to 20.0% at 0.10 wt%, reached the maximum value of 30.0% at 0.15 wt%, and then decreased to 22.0% at 0.20 wt% (Figure 8b). The permeability enhancement showed a similar optimum near 0.15 wt%, increasing from 224.65% at 0.05 wt% to 424.40% at 0.10 wt%, reaching 1708.33% at 0.15 wt%, and then decreasing to 783.67% at 0.20 wt% (Figure 8c). These results suggest that 0.15 wt% may represent the most favorable concentration for Agent 2 within the tested range.

Comparison between the two agent systems further demonstrates that Agent 2 achieved higher final recovery than Agent 1 at all tested concentrations (Figure 8b). This difference cannot be fully explained by the initial fractal dimension alone because the two agent systems had overlapping $D_{f,0}$ values at several concentrations. Instead, the recovery difference reflects the coupled control of fractal pore heterogeneity and interfacial regulation pathway. Agent 2 reduced the oil–water interfacial tension more effectively while maintaining a favorable apparent contact angle, which may facilitate reduction in oil–water interfacial resistance and improve access to connected larger pore–fracture domains and microfracture-related domains more efficiently. In contrast, Agent 1 mainly altered apparent wettability, and the associated increase in contact angle limited its ability to continuously improve oil recovery. The small variation in D_f before and after imbibition indicates that pressurized shut-in imbibition did not uniformly reconstruct the entire pore-size distribution. Rather, the major recovery and permeability responses were likely caused by selective

activation of accessible pore–fracture pathways within an already heterogeneous fractal pore system.

3.5. NMR-Based Pore-Size-Dependent Recovery

Time-lapse NMR T_2 spectra show that the oil signal decreased progressively during shut-in imbibition (Figure 7). The signal reduction was mainly concentrated around the dominant T_2 peak and the long-T_2 tail, indicating that oil was mobilized from both matrix pores and larger connected pore–fracture spaces. However, the magnitude of signal reduction differed among cores, which is consistent with the variation in total recovery shown in Figure 6. The stacked pore-size-dependent recovery contributions further reveal that total recovery was dominated by pores larger than 20 nm (Figure 9). For all eight cores, the >20 nm domain provided the largest contribution to total recovery at 144 h. This contribution was especially pronounced in the Agent 2 samples. H-7# treated with A2-0.15 showed the highest total contribution, mainly because of the large contribution from the >20 nm domain. H-8# treated with A2-0.20 and H-6# treated with A2-0.10 also showed high contributions from the >20 nm domain. By contrast, the <5 nm, 5–10 nm, and 10–20 nm domains contributed much less to total recovery. The internal mobilization degree M_i provides a different perspective by normalizing the recovered oil in each pore-size domain to its initial oil signal (Figure 9). For Agent 1, the internal mobilization degrees were generally low to moderate across all pore-size domains. A1-0.10 showed higher mobilization than A1-0.05, A1-0.15, and A1-0.20, consistent with its higher total recovery. For Agent 2, the internal mobilization degree increased markedly, especially in the <5 nm, 5–10 nm, and 10–20 nm domains for A2-0.10 and A2-0.15. This indicates that Agent 2 not only enhanced recovery from larger pores, but also improved the relative mobilization of some smaller pore-size domains.

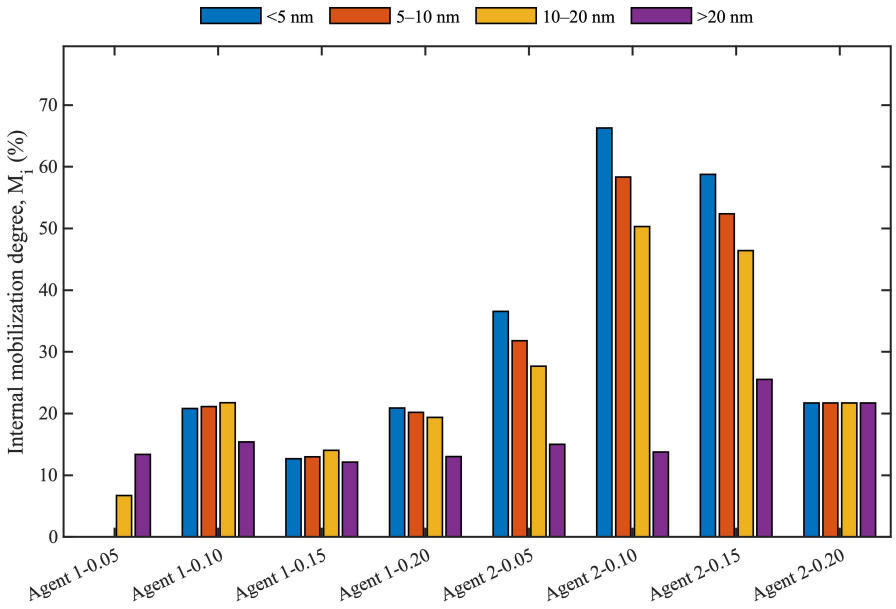


Figure 9. Pore-size-dependent oil recovery after 144 h of shut-in imbibition, showing the contribution of each pore-size domain to total recovery and the internal mobilization degree of each pore-size domain.

3.5.1. Oil Mobilization in Pores Smaller than 5 nm

The <5 nm domain made only a small contribution to total recovery in most samples, as shown by the limited blue portion in Figure 9. Although some Agent 2 samples showed relatively high internal mobilization degree in this domain, its contribution to total recovery remained limited because the initial recoverable oil volume in this domain was small or

because the connectivity was weak. This indicates that oil in the smallest nanopores was difficult to convert into substantial bulk recovery during the tested shut-in period.

3.5.2. Oil Mobilization in 5–10 nm Pores

The 5–10 nm domain showed a slightly stronger contribution than the <5 nm domain, but it was still secondary relative to larger pores. Agent 2, particularly A2-0.10 and A2-0.15, produced higher internal mobilization degrees in this interval than Agent 1. This suggests that interfacial regulation can improve the relative mobilization of 5–10 nm pores, but the contribution of this interval to total recovery remains constrained by pore-throat connectivity and limited storage volume.

3.5.3. Oil Mobilization in 10–20 nm Pores

The 10–20 nm domain contributed more noticeably to recovery than the two smaller nanopore domains. In the Agent 2 samples, especially A2-0.10 and A2-0.15, the internal mobilization degree in the 10–20 nm interval was relatively high. This pore-size interval can therefore be regarded as a transition domain where capillary-force regulation begins to translate more effectively into measurable oil recovery. The response of this domain is important because it links nanopore-confined oil storage with larger connected pore–fracture pathways.

3.5.4. Oil Mobilization in Pores Larger than 20 nm and Microfractures

The >20 nm domain was the dominant contributor to total recovery for all tested cores. This pore-size range includes larger pores, bedding-related pore spaces, and microfracture-associated flow pathways. The high contribution from this domain indicates that shut-in imbibition preferentially mobilized oil from relatively accessible and better-connected storage spaces. In several samples, especially H-6#, H-7#, and H-8#, the large contribution from the >20 nm domain controlled the final high total recovery.

Taken together, the time-lapse NMR spectra and pore-size-resolved recovery calculations demonstrate that shut-in imbibition in LGS shale is strongly pore-size selective. The total recovery is primarily controlled by the >20 nm domain, whereas smaller nanopores contribute less to bulk recovery despite showing some internal mobilization under favorable fluid conditions.

3.6. Apparent Nanopore Mobilization Threshold

The pore-size-dependent recovery curves reveal a clear contrast between nanopore-confined oil and oil stored in larger pores or microfracture-related spaces (Figure 10). For all eight LGS shale cores, the recovery contribution from pores larger than 20 nm dominated the total NMR-derived recovery throughout shut-in imbibition. In contrast, the contributions from the <5 nm, 5–10 nm, and 10–20 nm pore-size domains remained much smaller, even after 144 h. This indicates that oil mobilization during shut-in imbibition was not uniformly distributed across the pore-size spectrum. For the Agent 1 system, the >20 nm domain was the primary contributor to recovery in all tested concentrations. The cumulative recovery in H-1# to H-4# increased mainly through the expansion of the >20 nm contribution, whereas the smaller pore-size domains showed only limited growth. Even when total recovery increased substantially, particularly in H-2#, H-3#, and H-4#, the increase was still mainly controlled by the large-pore and microfracture-related domain. This suggests that Agent 1 promoted oil mobilization primarily from accessible connected pores rather than from the smallest nanopores. A similar pattern was observed for the Agent 2 system. In H-5# to H-8#, the >20 nm pore-size domain contributed the largest proportion of recovery, especially during the middle and late shut-in stages. The 10–20 nm domain showed some contribution and became more visible in several samples, but its

contribution remained secondary compared with the >20 nm domain. The <5 nm and 5–10 nm intervals contributed only a small fraction of the total recovery, confirming that the smallest nanopores were difficult to mobilize under the tested shut-in conditions. These results indicate an apparent mobilization threshold near 20 nm. Pores smaller than approximately 20 nm were not completely inactive, but their contribution to total recovery was limited within the 144 h shut-in period. In contrast, pores larger than 20 nm showed a much stronger and more sustained recovery response. Therefore, the threshold should be interpreted as an apparent experimental mobilization threshold rather than an absolute physical boundary. The apparent threshold reflects the combined effects of capillary pressure, wettability, oil occurrence state, pore-throat connectivity, and imbibition-agent accessibility. Although smaller nanopores may have high calculated capillary pressure, high capillary pressure alone does not guarantee efficient oil release. Oil in nanopores may be strongly adsorbed on organic or clay-rich surfaces, and the pore network may be poorly connected. In addition, imbibition-agent molecules may have limited access to the smallest pore throats. These constraints limit the conversion of capillary-force regulation into effective nanopore oil recovery.

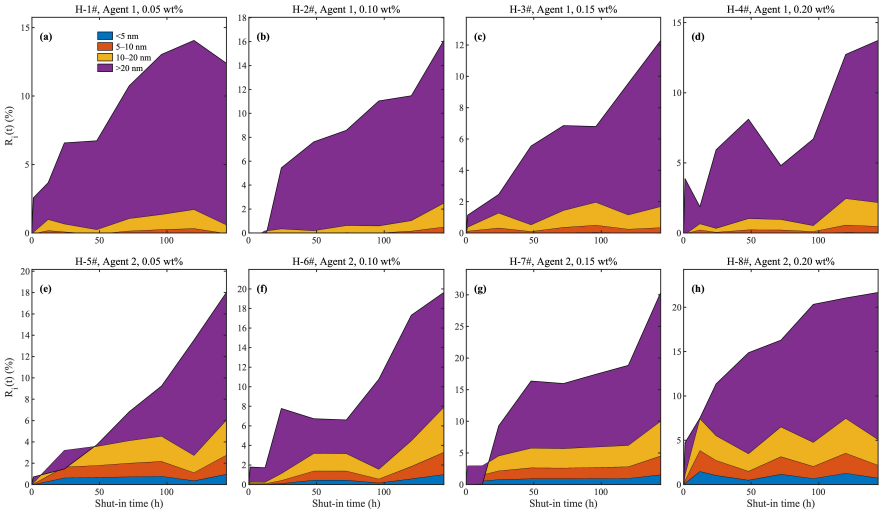


Figure 10. Evolution of pore-size-dependent recovery during shut-in imbibition, showing the dominant contribution of pores larger than 20 nm and the apparent nanopore mobilization threshold near 20 nm. (**a**) H-1#, Agent 1, 0.05 wt%; (**b**) H-2#, Agent 1, 0.10 wt%; (**c**) H-3#, Agent 1, 0.15 wt%; (**d**) H-4#, Agent 1, 0.20 wt%; (**e**) H-5#, Agent 2, 0.05 wt%; (**f**) H-6#, Agent 2, 0.10 wt%; (**g**) H-7#, Agent 2, 0.15 wt%; (**h**) H-8#, Agent 2, 0.20 wt%.

Overall, Figure 10 shows that shut-in imbibition in LGS shale mainly mobilized oil from the >20 nm pore-size domain and connected microfracture-related spaces. Future imbibition-agent design should therefore not only reduce interfacial tension or alter wettability, but also improve access to poorly connected nanopores and promote the activation of effective flow pathways.

3.7. Pore Enlargement and Microfracture Activation After Imbibition

Visual comparison before and after shut-in imbibition provides direct evidence that the imbibition process modified the internal flow pathways of selected LGS shale cores (Figure 11). For both Agent 1 and Agent 2 systems, the post-imbibition images show more continuous and vertically developed red-stained pathways than those observed before imbibition. Before imbibition, the stained regions were generally discrete, spot-like, or weakly connected, indicating limited initial connectivity of the pore–fracture system. After imbibition, the stained regions became more continuous and extended along preferential

pathways, suggesting that shut-in imbibition promoted the activation or enlargement of connected pore–fracture channels. For Agent 1, the samples treated at 0.10 wt%, 0.15 wt%, and 0.20 wt% all showed visible enhancement of connected stained pathways after imbibition. The post-imbibition images show that originally scattered pore-scale or fracture-scale signals evolved into more continuous streak-like features. This indicates that Agent 1 not only mobilized oil through wettability regulation, but also facilitated fluid penetration along pre-existing weak planes, bedding-related discontinuities, or microfractures. The response was especially evident in the 0.10 wt% and 0.20 wt% cases, where post-imbibition staining became more vertically connected. For Agent 2, a similar but slightly different structural response was observed. The 0.10 wt%, 0.15 wt%, and 0.20 wt% samples showed stronger connected red-stained zones after imbibition, with more evident continuous pathways than before imbibition. The 0.15 wt% case showed a particularly clear transformation from a weakly stained pre-imbibition state to a strongly connected post-imbibition pathway. This result suggests that Agent 2 promoted the development of effective flow pathways, likely through combined interfacial tension reduction and wettability regulation. The visual evidence is consistent with the NMR and permeability results. The increase in long-T_2 components after imbibition indicates enhanced large-pore or microfracture-related signals, while the post-imbibition dry-core permeability increase confirms that the improvement was not only a temporary liquid-saturation effect. Therefore, the combined visual, NMR, and permeability evidence suggests that shut-in imbibition can induce persistent modification of the connected pore–fracture system in LGS shale.



Figure 11. Visual evidence for imbibition-induced pore enlargement and microfracture activation in LGS shale cores treated with different concentrations of Agent 1 and Agent 2.

It should be noted that the observed structural response does not imply uniform fracture generation in all pores. Instead, the images indicate preferential activation and enlargement of existing weak flow paths. The imbibition fluid likely entered along bedding-related discontinuities, microfractures, and relatively larger connected pores, thereby improving local connectivity and producing the observed permeability enhancement. This heterogeneous response explains why the post-imbibition permeability increase varied significantly among cores and concentrations.

3.8. Permeability Evolution After Shut-In Imbibition

The permeability response after shut-in imbibition showed a clear enhancement trend for all tested LGS shale cores, although the magnitude of enhancement varied substantially among samples and imbibition-agent concentrations (Figure 12). The dry-core permeability measured at 10 MPa increased after imbibition in every case, indicating that the permeabil-

ity improvement was not a transient effect caused by residual liquid saturation, but was associated with persistent modification of the connected pore–fracture system. For Agent 1, the permeability enhancement was strongly concentration-dependent. The lowest concentration, A1-0.05, produced only a slight increase in permeability, with an enhancement ratio of 6.70%. In contrast, A1-0.10 resulted in the largest enhancement among all tested samples, with permeability increasing from 0.01061 mD to 0.2538 mD and an enhancement ratio of 2292.08%. A1-0.15 and A1-0.20 also produced substantial permeability increases, with enhancement ratios of 1257.14% and 1344.75%, respectively. These results indicate that Agent 1 can markedly improve post-imbibition flow capacity once an effective concentration is reached, although the response is not strictly monotonic with concentration. For Agent 2, all concentrations also resulted in permeability enhancement. The permeability increased from 0.03875 mD to 0.1258 mD for A2-0.05, from 0.08324 mD to 0.43651 mD for A2-0.10, from 0.0036 mD to 0.0651 mD for A2-0.15, and from 0.0294 mD to 0.2598 mD for A2-0.20. The corresponding enhancement ratios were 224.65%, 424.40%, 1708.33%, and 783.67%, respectively. Compared with Agent 1, Agent 2 produced a consistently positive permeability response over the full concentration range, but the maximum enhancement was observed at A2-0.15 rather than at the highest concentration. The enhancement ratios were much larger in cores with very low initial permeability, especially H-2#, H-3#, and H-7#. This suggests that the relative permeability increase may be influenced by the imbibition-agent type and concentration, but also by the initial pore–fracture structure of the core. Samples with initially poor flow capacity may be more sensitive to pore-throat enlargement, bedding-interface opening, or microfracture activation during shut-in imbibition. In contrast, samples with relatively higher initial permeability showed smaller relative enhancement because their initial connected flow pathways were already more developed. Overall, Figure 12 demonstrates that shut-in imbibition improved the dry-core permeability of all tested LGS shale samples, but the enhancement was highly heterogeneous. This heterogeneity suggests that post-imbibition permeability evolution is jointly controlled by capillary-force regulation, initial pore–fracture connectivity, bedding-related discontinuities, and the extent of imbibition-induced structural modification. Therefore, the potential benefit of shut-in imbibition should be evaluated not only from total oil recovery, but also from the resulting change in connected flow capacity after imbibition.

3.9. Unified Fractal–Transport Coupling Framework

To quantitatively address the coupling between fractal pore heterogeneity and transport behavior, Pearson and Spearman correlation analyses were performed between the NMR-derived fractal dimension (D_f), oil recovery, and permeability enhancement. The results show that D_f exhibits a weak but consistent positive correlation with recovery, while a stronger nonlinear correlation is observed between D_f and permeability enhancement. Cross-plot analysis further confirms distinct scaling behaviors. A linear regression is observed between D_f and recovery, indicating a weak direct control of fractal complexity on total imbibition efficiency. In contrast, permeability enhancement follows a power-law relationship with D_f in log–log space, suggesting a fractal-controlled transport regime dominated by connected pore–fracture activation rather than bulk pore reconstruction. The ΔD_f–recovery relationship shows no strong linear dependence, indicating that fractal evolution during shut-in imbibition is localized and does not represent global restructuring of the pore system. This supports the interpretation that imbibition primarily activates pre-existing high-connectivity pathways rather than modifying the entire fractal network. Although a full multifractal analysis is not performed due to the limited signal resolution of the T_2 distribution, the observed nonlinear scaling behavior and heterogeneous permeability response suggest the presence of implicit multifractal characteristics in the

pore–fracture system. This limitation is acknowledged and will be addressed in future work using higher-resolution NMR or μ-CT datasets.

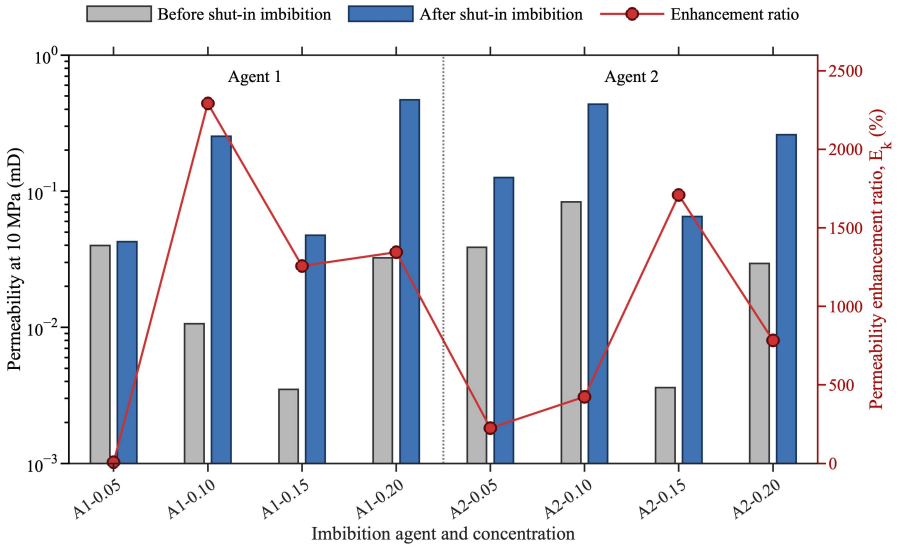


Figure 12. Permeability change before and after shut-in imbibition under different imbibition-agent concentrations.

The unified framework (Figure 13) demonstrates that fractal pore heterogeneity controls transport response in a weakly coupled but statistically identifiable manner, with permeability evolution exhibiting stronger fractal dependence than total oil recovery.

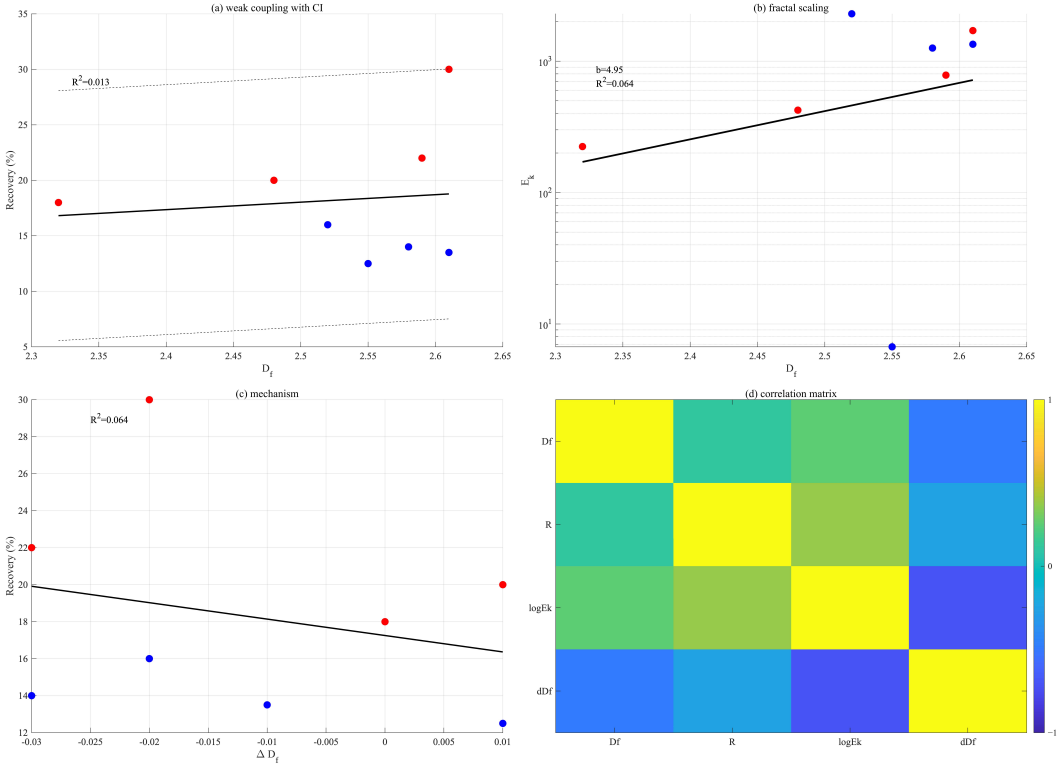


Figure 13. Integrated fractal–structure–transport coupling framework for capillary-force-regulated shut-in imbibition and permeability evolution in heterogeneous shale oil systems. Red dots represent the observations for Agent 2, blue dots represent the observations for Agent 1, black solid lines indicate the fitted relationships, and black dashed lines denote weak or conceptual coupling trends. The framework summarizes the statistically identifiable coupling among fractal pore heterogeneity, pore-scale transport, oil recovery, and permeability evolution during shut-in imbibition.

4. Discussion

4.1. Fractal Control on Concentration-Dependent Shut-In Imbibition

The NMR-derived fractal analysis provides a structural basis for understanding why the two imbibition agents produced different concentration-dependent recovery and permeability responses. The relatively high clay content (34–50%) suggests that adsorption-related and surface-interaction effects may contribute to fluid retention behavior; however, these effects operate in conjunction with pore-size-dependent capillary forces and connectivity constraints in a strongly heterogeneous fractal pore system. The LGS shale oil cores exhibited D_f values mainly between 2.3 and 2.6, confirming that the pore system has strong multiscale heterogeneity. In such a pore system, oil is stored not only in larger connected pores and microfractures but also in nanopores and transition pores with different degrees of accessibility. Therefore, shut-in imbibition is controlled not only by capillary pressure but also by whether the imbibition fluid can effectively enter the connected pore–fracture network. The interpretation of imbibition behavior is constrained by measured XRD mineralogical data, which indicate a clay-rich and quartz-dominated shale system.

The interfacial measurements show that Agent 1 and Agent 2 represent two different capillary-force regulation pathways. Agent 1 moderately reduced the oil–water interfacial tension from 31.85 to 27.20 mN/m, but increased the apparent contact angle from 51.0° to 66.1°. The larger apparent contact angle reduced $\cos\theta$, and therefore decreased the effective capillary-force term $\sigma\cos\theta$ to 11.02 mN/m. This indicates that Agent 1 mainly acted through apparent wettability alteration. However, for a highly heterogeneous fractal pore system, reducing the capillary-force term does not necessarily improve oil recovery from all pore-size domains. If the imbibition fluid cannot effectively enter poorly connected nanopores or if oil remains adsorbed on organic or clay-related surfaces, apparent wettability alteration alone may have limited recovery benefit.

Agent 2 showed different behavior. It reduced the oil–water interfacial tension more strongly from 31.85 to 22.12 mN/m while maintaining a favorable apparent contact angle of 49.3°. Although its $\sigma\cos\theta$ value was not the lowest among the tested fluids, Agent 2 provided a more favorable balance between interfacial tension reduction and wettability condition. This balance is important because oil mobilization in LGS shale requires both reduced oil–water interfacial resistance and sufficient accessibility of connected pore throats and microfracture-related spaces. Therefore, Agent 2 more effectively converted the fractal pore structure into recoverable oil pathways, which explains its higher final recovery at all tested concentrations.

The optimum response of Agent 2 at 0.15 wt% further indicates that the relationship between agent concentration and imbibition performance is non-monotonic. At low concentration, the amount of active component may be insufficient to fully regulate the oil–water interface and fluid–rock interface within the complex pore network. At moderate concentration, interfacial tension reduction and favorable wettability condition jointly improve the accessibility of connected pore–fracture domains, leading to higher recovery and stronger permeability enhancement. At excessive concentrations, further additive increase may not improve access to isolated nanopores and may even cause adsorption loss, interfacial aggregation, or an unfavorable redistribution of the capillary driving force. Therefore, 0.15 wt% represents the most favorable balance between interfacial tension reduction, apparent wettability condition, and pore–fracture accessibility for Agent 2 in the tested LGS shale cores.

The small changes in D_f after imbibition are also important. The recovery and permeability enhancement changed substantially with concentration, whereas the global fractal dimension changed only slightly. This suggests that pressurized shut-in imbibition did not uniformly reconstruct the entire pore system. Instead, it selectively activated or enlarged

preferential pathways, including larger pores, bedding-related voids, and microfracture-associated spaces. This interpretation is consistent with the pore-size-dependent recovery results, which show that pores larger than 20 nm dominated total recovery, whereas pores smaller than 20 nm contributed only limited recovery. Therefore, the apparent nanopore mobilization threshold near 20 nm can be understood as the result of fractal pore heterogeneity, limited nanopore connectivity, oil adsorption, and restricted molecular accessibility of imbibition agents.

Overall, the fractal analysis indicates that the LGS shale pore system provides a heterogeneous structural framework for shut-in imbibition, but the final recovery and permeability enhancement depend on how effectively the imbibition agent converts this structural heterogeneity into accessible flow pathways. Agent 2 was more effective because its interfacial regulation pathway reduced oil–water interfacial resistance while maintaining a favorable apparent wettability condition, thereby promoting oil mobilization from connected pore–fracture domains without requiring a large change in the global fractal dimension. Thus, effective imbibition-agent design for continental shale oil reservoirs should not only target interfacial tension reduction or wettability alteration individually, but should optimize the combined effects of interfacial tension reduction, apparent wettability, pore accessibility, and microfracture activation within a multiscale fractal pore system. The concentration-dependent trends presented in this study should be interpreted as qualitative behavioral trends rather than statistically validated relationships.

4.2. Coupled Mechanism of Surfactant-Assisted Shut-In Imbibition

The results indicate that surfactant-assisted shut-in imbibition in LGS shale is governed by a coupled interfacial–capillary–pore-structure mechanism rather than by a single fluid-property parameter. After the imbibition agents were added to the base fracturing fluid, the oil–water interfacial tension and apparent contact angle changed simultaneously. The integrated conceptual mechanism summarizing these coupled processes is illustrated in Figure 14. These changes modified the effective capillary-force term $\sigma\cos\theta$, thereby altering the capillary pressure distribution across different pore-size domains. The calculated capillary pressure curves show that this regulation was most sensitive in nanopore-scale domains, but the NMR-derived recovery results demonstrate that the actual oil recovery was mainly contributed by pores larger than 20 nm and microfracture-related spaces. A conceptual mechanism can therefore be proposed as follows. First, the imbibition agent reduces the oil–water interfacial tension and/or alters the apparent wettability of the oil-aged shale surface. Second, the modified interfacial properties change the capillary pressure distribution and reduce the resistance for the imbibition fluid to enter accessible pore throats and microfractures. Third, during pressurized shut-in, the imbibition fluid preferentially invades connected larger pores, bedding-related microfractures, and weakly cemented pore–fracture pathways. Fourth, oil in these relatively accessible domains is displaced or redistributed, leading to a reduction in the NMR T_2 signal amplitude and an increase in calculated oil recovery. Finally, in selected cores, continued fluid–rock interaction and pressure-assisted imbibition further activate weak flow paths, producing pore enlargement, microfracture reconnection, and post-imbibition permeability enhancement. This coupled mechanism explains why Agent 2 generally achieved higher total recovery than Agent 1. Agent 2 produced a stronger interfacial tension reduction while maintaining a relatively favorable apparent contact angle, resulting in more effective capillary-force regulation for accessible pore systems. By contrast, Agent 1 produced a stronger apparent wettability change but a lower $\sigma\cos\theta$ value, leading to a different capillary pressure response. Therefore, the performance of an imbibition agent should be evaluated through the combined effects of interfacial tension, apparent contact angle, capillary pressure response, pore-size-dependent

recovery, and post-imbibition permeability evolution. It should be emphasized that the calculated capillary pressures are used as comparative indicators to evaluate the relative capillary-force regulation among different imbibition fluids across pore-size domains. They do not represent the actual pore-scale capillary pressures within the complex and heterogeneous shale pore system.

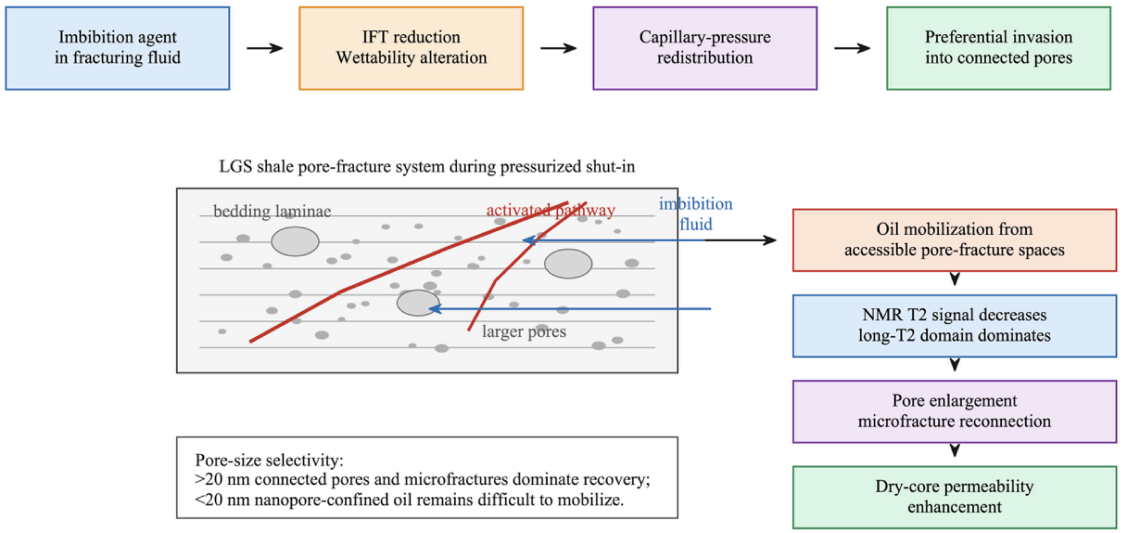


Figure 14. Conceptual mechanism of surfactant-assisted pressurized shut-in imbibition in LGS shale.

4.3. Why Small Pores Remain Difficult to Mobilize

A key finding of this study is that oil recovery from pores smaller than approximately 20 nm remained limited during the 144 h shut-in period, even though the calculated capillary pressure in these pore-size domains was high. This indicates that shut-in imbibition is not controlled only by the thermodynamic reduction in interfacial tension, but also by molecular accessibility, pore-throat connectivity, and the residence state of oil in nanopores. First, small pores impose strong interfacial confinement. In the <5 nm and 5–10 nm domains, the surface-to-volume ratio is extremely high, and the oil–water interface is strongly affected by wall interaction. Although classical capillary theory predicts high capillary pressure in small pores, the actual displacement process can be restricted by the narrow pore-throat geometry and local wetting heterogeneity. As a result, high capillary pressure does not necessarily translate into efficient oil displacement. Second, oil in nanopores may exist in a strongly adsorbed or semi-adsorbed state. Organic matter pores, clay-related nanopores, and mineral surface-associated pores can retain oil through adsorption, polar interactions, and confinement effects. This type of oil is less mobile than oil stored in larger pores or microfractures. Therefore, even when the imbibition fluid modifies interfacial properties, the oil in nanopores may remain difficult to detach from the pore surface. Third, the molecular accessibility of imbibition agents is limited in nanopore systems. Surfactant or imbibition-agent molecules must enter pore throats and reach the oil–solid or oil–water interface to exert their effect. In very small pores, steric restriction, adsorption loss, and pore-throat blockage may reduce the effective concentration of the active agent. This limits the ability of the agent to alter wettability or reduce interfacial resistance at the actual oil-storage location. Fourth, the shut-in duration may be insufficient for effective nanopore-scale diffusion. The experimental results show that recovery increased rapidly at early times and then slowed, suggesting that accessible large pores and connected microfractures were mobilized first. Oil stored in poorly connected nanopores requires longer diffusion paths and slower mass transfer. Within the 144 h experimental period, this oil

could not be substantially converted into bulk recovery. This apparent threshold can be further interpreted as a capillary-entry accessibility constraint, where pore-throat geometry, interfacial pressure barrier, and molecular transport limitation collectively control whether capillary-driven imbibition can be effectively translated into recoverable oil.

Therefore, the apparent mobilization threshold near 20 nm should not be interpreted as a fixed physical boundary. Instead, it reflects the combined effects of pore size, pore connectivity, oil occurrence state, fluid accessibility, and shut-in duration. This threshold provides an important criterion for evaluating whether a given imbibition agent can effectively access and mobilize nanopore-confined oil in continental shale reservoirs.

4.4. Imbibition-Induced Pore Enlargement and Microfracture Activation

The visual observations, NMR response, and post-imbibition permeability results jointly indicate that pressurized shut-in imbibition can modify the connected pore–fracture system of LGS shale. The post-imbibition images show more continuous red-stained pathways than those before imbibition, suggesting that the imbibition fluid preferentially entered and enlarged pre-existing weak pathways. Meanwhile, the NMR results show enhanced contribution from long-T_2 domains, and the dry-core permeability increased after imbibition in all tested samples. These results support the interpretation that shut-in imbibition can promote pore enlargement and microfracture activation under favorable conditions. The proposed mechanism is that, during pressurized shut-in, the imbibition fluid first enters bedding-related discontinuities, microfractures, and connected larger pores. These pathways are more accessible than isolated nanopores and provide preferential channels for fluid invasion. As imbibition proceeds, fluid–rock interaction may weaken mineral interfaces, bedding contacts, or clay-rich laminae. Local hydration, interfacial weakening, and pressure-assisted fluid penetration may reopen previously closed microfractures or enlarge narrow pore throats. Once these weak paths are reconnected, the effective flow capacity increases, which is reflected by the higher dry-core permeability after imbibition. This process is consistent with the permeability data. Samples with very low initial permeability, such as H-2#, H-3#, and H-7#, showed particularly large relative permeability enhancement. These cores may initially contain poorly connected but activatable pore–fracture networks. Once shut-in imbibition opened or reconnected part of these weak pathways, the relative increase in permeability became large. By contrast, samples with higher initial permeability showed smaller relative enhancement because their flow pathways were already more developed before imbibition. However, pore enlargement and microfracture activation should not be regarded as uniform fracture generation throughout the shale matrix. The evidence points to preferential activation of existing weak structural planes rather than homogeneous creation of new fractures. The degree of enhancement depends on initial bedding development, natural microfracture abundance, mineral composition, clay sensitivity, and the local stress state. Therefore, pressurized shut-in imbibition may improve permeability in some shale cores, but the magnitude of improvement is expected to be heterogeneous.

This finding is important because shut-in imbibition has traditionally been evaluated mainly from oil recovery or retained-fluid damage. The present results show that, in LGS shale, shut-in imbibition may also act as a pore–fracture reconstruction process. The final production benefit may therefore depend on the balance between oil displacement, liquid retention, and structural modification of the pore–fracture network.

4.5. Implications for Shut-In Operation and Imbibition-Agent Design

The results provide several implications for shut-in operation and imbibition-agent design in LGS continental shale oil reservoirs. First, Agent 2 is more suitable for the tested

LGS shale cores than Agent 1 from the perspective of total recovery, pore-size-dependent mobilization, and permeability enhancement. Agent 2 generally produced higher total recovery, stronger mobilization in multiple pore-size domains, and consistently positive post-imbibition permeability response. Based on the present experimental results, concentrations higher than 0.10 wt% are preferable for Agent 2, with A2-0.15 showing the strongest recovery response among the tested conditions. However, the concentration effect was not strictly monotonic, so optimization should consider both recovery and permeability response rather than only additive dosage. Second, shut-in time should not be determined only from total recovery. The recovery curves show an early rapid stage, an intermediate slow stage, and a late-stage plateau or continued increase. More importantly, the pore-size-dependent recovery results indicate that the >20 nm domain dominates recovery, while smaller pores contribute much less. Therefore, shut-in duration should be evaluated using both total recovery and pore-size-resolved recovery. When the contribution from accessible pore-size domains approaches a plateau, extending shut-in time may provide limited additional recovery unless structural activation or deeper pore access occurs. Third, conventional imbibition agents are still insufficient for effectively mobilizing oil from pores smaller than approximately 20 nm. Future agent design should focus on improving nanopore accessibility, reducing adsorption loss, and enhancing molecular-scale oil detachment. Small-molecule, low-adsorption, low-retention, and nanopore-accessible imbibition agents may be more effective for mobilizing oil from clay-related and organic nanopores. In addition, formulations should be designed to maintain activity after entering narrow pore throats rather than only showing favorable bulk interfacial properties. Fourth, imbibition-agent development should balance oil-displacement capacity with pore–fracture modification and formation-damage risk. The present results show that shut-in imbibition can enhance permeability through pore enlargement and microfracture activation. However, excessive fluid–rock interaction may also cause clay swelling, particle migration, fines release, or pore-throat blockage in sensitive cores. Therefore, future formulations should aim to promote controlled pore–fracture connectivity enhancement while avoiding excessive hydration damage or instability of the shale matrix.

Overall, the optimal shut-in strategy for LGS shale should integrate capillary-force regulation, pore-size-dependent recovery, and post-imbibition permeability evolution. A suitable imbibition agent should not only improve bulk oil recovery, but also access effective pore-size domains, preserve or enhance flow pathways, and minimize long-term formation damage. In response to concerns regarding data usability and compositional transparency, it should be emphasized that while proprietary constraints limit disclosure of exact surfactant formulations, all key interfacial properties governing imbibition behavior (IFT, contact angle, and $\sigma\cos\theta$) are fully reported. These parameters are widely recognized as primary descriptors of capillary-force regulation and therefore provide a reproducible framework for comparing imbibition performance across different systems.

A key limitation of this study is the lack of experimental replication for each concentration. Therefore, statistical significance testing (e.g., ANOVA or t-tests) could not be performed. Future studies should include replicated core-scale experiments to improve statistical robustness. Due to the absence of TOC, thermal maturity, and kerogen type measurements for the studied samples, organic matter-related effects are not quantitatively evaluated in this work. Therefore, mechanistic interpretations related to oil occurrence are primarily based on mineralogy-controlled pore structure and capillary-force-driven imbibition processes.

4.6. Origin of the Extremely High Permeability Enhancement

The extremely high permeability enhancement observed in this study (up to 1708%) is primarily attributed to imbibition-induced activation of connected pore–fracture pathways rather than a proportional increase in matrix permeability. The initial permeability of the LGS shale cores is extremely low (0.003–0.08 mD), indicating a near-disconnected flow system. In such ultra-low-permeability media, even minor structural reconnection of pre-existing microfractures, bedding-related discontinuities, or weak pore-throat pathways can lead to orders-of-magnitude increases in effective flow capacity. Post-imbibition CT images and NMR T_2 spectrum shifts confirm that pressurized shut-in imbibition selectively enhances connectivity in larger pores and microfracture-associated domains, rather than uniformly modifying the entire pore network. Therefore, the reported permeability increase should be interpreted as a connectivity-controlled flow regime transition rather than a linear permeability improvement of the rock matrix.

In this context, the large percentage increase reflects the extremely low baseline permeability and the emergence of newly connected flow channels during imbibition. This interpretation is consistent with the heterogeneous nature of the LGS shale pore–fracture system and the fractal pore architecture identified in this study.

5. Conclusions

This study investigated capillary-force-regulated pressurized shut-in imbibition in LGS continental shale oil cores by integrating interfacial tension measurements, apparent contact angle tests, capillary pressure calculation, time-lapse NMR monitoring, NMR-based fractal characterization, visual observations, and pre-/post-imbibition permeability measurements. The main conclusions are as follows.

(1) NMR-derived fractal analysis confirmed the multiscale and heterogeneous pore structure of LGS continental shale oil cores. The initial fractal dimension D_{f,0} mainly ranged from approximately 2.32 to 2.61, indicating that the T_2-derived pore-size distribution was controlled by a complex pore system consisting of nanopores, transition pores, larger pores, bedding-related voids, and microfracture-associated spaces. The limited variation between the initial and final fractal dimensions suggests that pressurized shut-in imbibition did not uniformly reconstruct the entire pore-size distribution, but preferentially affected accessible pore–fracture pathways within an already heterogeneous fractal pore system.

(2) Agent 1 and Agent 2 regulated shut-in imbibition through different interfacial and wettability pathways. Agent 1 moderately reduced the oil–water interfacial tension from 31.85 to 27.20 mN/m but increased the apparent contact angle from 51.0° to 66.1°, indicating a dominant apparent-wettability-alteration effect. In contrast, Agent 2 reduced the interfacial tension more strongly to 22.12 mN/m while maintaining a favorable apparent contact angle of 49.3°. This more balanced interfacial regulation allowed Agent 2 to reduce oil–water interfacial resistance while preserving favorable access to connected pore–fracture domains.

(3) The concentration-dependent imbibition response showed that Agent 2 outperformed Agent 1 in terms of oil recovery. For Agent 1, the final recovery reached a relatively high value of 16.0% at 0.10 wt% but remained low at higher concentrations. For Agent 2, recovery increased from 18.0% at 0.05 wt% to a maximum of 30.0% at 0.15 wt%, followed by a decrease to 22.0% at 0.20 wt%. Therefore, 0.15 wt% was identified as the most effective concentration for Agent 2 within the tested range. The recovery improvement was not controlled by fractal dimension alone, but by the coupling of fractal pore heterogeneity, interfacial tension reduction, apparent wettability, pore-throat accessibility, and microfracture activation.

(4) Time-lapse NMR demonstrated that oil mobilization during pressurized shut-in imbibition was strongly pore-size-dependent. Pores larger than 20 nm, including larger pores, bedding-related spaces, and microfracture-associated storage domains, dominated the total recovery contribution. In contrast, the <5 nm, 5–10 nm, and 10–20 nm domains contributed much less to bulk recovery, although partial internal mobilization occurred under favorable fluid conditions. These results indicate an apparent nanopore mobilization threshold near 20 nm. This threshold is not an absolute physical boundary, but reflects the combined limitations imposed by fractal pore heterogeneity, pore-throat connectivity, oil adsorption, molecular accessibility of imbibition agents, and finite shut-in duration.

(5) Pressurized shut-in imbibition not only mobilized oil but also modified the connected pore–fracture system in LGS shale. Visual observations showed more continuous stained pathways after imbibition, while NMR responses indicated enhanced long-T_2 components associated with larger pores and microfracture-related spaces. Dry-core permeability increased after imbibition in all tested samples, but the enhancement was highly heterogeneous. Agent 2 showed a clearer optimum response at 0.15 wt%, with a permeability enhancement of 1708.33%. These results suggest that permeability improvement mainly resulted from selective pore-throat enlargement, bedding-interface opening, and microfracture activation, rather than uniform reconstruction of the global fractal pore system.

It should be noted that all concentration-dependent observations reported in this study represent system-specific experimental trends rather than statistically generalized or universally applicable relationships. Beyond the specific LGS shale samples investigated in this study, the results highlight a more general insight that shut-in imbibition in heterogeneous shale systems is primarily controlled by the coupling of interfacial regulation and pore–fracture connectivity, rather than by any single fluid-property parameter. The observed permeability enhancement and recovery behavior therefore reflect a connectivity-driven flow activation process that may be applicable to other multiscale shale reservoirs. However, the present study is limited by the lack of experimental replication for each concentration and the relatively small number of core samples. In addition, CT analysis was mainly used for qualitative interpretation without quantitative fracture network extraction or connectivity evaluation. Future research should focus on statistically validated core-scale experiments, quantitative micro-CT-based fracture and pore-network characterization, and integrated NMR–MICP or adsorption-calibrated pore-size analysis under true reservoir stress conditions to improve the generality and predictive capability of the proposed mechanism.

Author Contributions: Conceptualization, B.L. and H.L.; methodology, H.L. and B.L.; software, H.L.; validation, H.L. and B.L.; formal analysis, H.L.; investigation, H.L.; resources, B.L.; data curation, H.L.; writing—original draft preparation, H.L.; writing—review and editing, B.L. and H.L.; visualization, H.L.; supervision, B.L.; project administration, B.L.; funding acquisition, B.L. All authors have read and agreed to the published version of the manuscript.

Funding: This research was funded by the National Natural Science Foundation of China, Grant No. 52004308.

Data Availability Statement: The raw data supporting the conclusions of this article will be made available by the authors on request.

Conflicts of Interest: The authors declare no conflict of interest.

References

1. Zou, C.; Yang, Z.; Cui, J.; Zhu, R.; Hou, L.; Tao, S.; Yuan, X.; Wu, S.; Lin, S.; Wang, L. Formation mechanism, geological characteristics and development strategy of nonmarine shale oil in China. *Pet. Explor. Dev.* **2013**, *40*, 15–27. [CrossRef]

2. Pang, X.; Li, M.; Li, B.; Wang, T.; Hui, S.; Liu, Y.; Liu, G.; Hu, T.; Xu, T.; Jiang, F.; et al. Main controlling factors and movability evaluation of continental shale oil. *Earth-Sci. Rev.* **2023**, *243*, 104472. [CrossRef]
3. Xia, D.; Yang, Z.; Gao, T.; Li, H.; Lin, W. Characteristics of micro- and nano-pores in shale oil reservoirs. *J. Pet. Explor. Prod. Technol.* **2021**, *11*, 157–169. [CrossRef]
4. Loucks, R.G.; Reed, R.M.; Ruppel, S.C.; Jarvie, D.M. Morphology, genesis, and distribution of nanometer-scale pores in siliceous mudstones of the Mississippian Barnett Shale. *J. Sediment. Res.* **2009**, *79*, 848–861. [CrossRef]
5. Hu, Q.; Ewing, R.P.; Rowe, H.D. Low nanopore connectivity limits gas production in Barnett Formation. *J. Geophys. Res. Solid Earth* **2015**, *120*, 8073–8087. [CrossRef]
6. Rose, W. A note on the role played by sediment bedding in causing permeability anisotropy. *J. Pet. Technol.* **1983**, *35*, 330–332. [CrossRef]
7. Jiang, S.; Sun, H.; Fang, J.; Bao, H.; Shu, Z.; Li, J.; Ju, Y. Bedding-parallel fractures in shale: Formation mechanisms, geological significance, and implications for hydrocarbon accumulation—A review. *Earth-Sci. Rev.* **2026**, *277*, 105447. [CrossRef]
8. Backeberg, N.R.; Iacoviello, F.; Rittner, M.; Mitchell, T.M.; Jones, A.P.; Day, R.; Wheeler, J.; Shearing, P.R.; Vermeesch, P.; Striolo, A. Quantifying the anisotropy and tortuosity of permeable pathways in clay-rich mudstones using models based on X-ray tomography. *Sci. Rep.* **2017**, *7*, 14838. [CrossRef] [PubMed]
9. Qi, C.; Wang, X.; Wang, W.; Liu, J.; Tuo, J.; Liu, K. Three-dimensional characterization of micro-fractures in shale reservoir rocks. *Pet. Res.* **2018**, *3*, 259–268. [CrossRef]
10. Shaibu, R.; Guo, B. The dilemma of soaking a hydraulically fractured horizontal shale well prior to flowback—A decade literature review. *J. Nat. Gas Sci. Eng.* **2021**, *94*, 104084. [CrossRef]
11. Wijaya, N.; Sheng, J.J. Shut-in effect in removing water blockage in shale-oil reservoirs with stress-dependent permeability considered. *SPE Reserv. Eval. Eng.* **2020**, *23*, 81–94. [CrossRef]
12. Dehghanpour, H.; Lan, Q.; Saeed, Y.; Fei, H.; Qi, Z. Spontaneous imbibition of brine and oil in gas shales: Effect of water adsorption and resulting microfractures. *Energy Fuels* **2013**, *27*, 3039–3049. [CrossRef]
13. Washburn, E.W. The dynamics of capillary flow. *Phys. Rev.* **1921**, *17*, 273–283. [CrossRef]
14. Mason, G.; Morrow, N.R. Developments in spontaneous imbibition and possibilities for future work. *J. Pet. Sci. Eng.* **2013**, *110*, 268–293. [CrossRef]
15. Alvarez, J.O.; Schechter, D.S. Wettability alteration and spontaneous imbibition in unconventional liquid reservoirs by surfactant additives. *SPE Reserv. Eval. Eng.* **2017**, *20*, 107–117. [CrossRef]
16. Sheng, J.J. What type of surfactants should be used to enhance spontaneous imbibition in shale and tight reservoirs? *J. Pet. Sci. Eng.* **2017**, *159*, 635–643. [CrossRef]
17. Xu, D.; Bai, B.; Wu, H.; Hou, J.; Meng, Z.; Sun, R.; Li, Z.; Lu, Y.; Kang, W. Mechanisms of imbibition enhanced oil recovery in low permeability reservoirs: Effect of IFT reduction and wettability alteration. *Fuel* **2019**, *244*, 110–119. [CrossRef]
18. Coates, G.R.; Xiao, L.; Prammer, M.G. *NMR Logging: Principles and Applications*; Halliburton Energy Services: Houston, TX, USA, 1999.
19. Guo, J.; Li, M.; Chen, C.; Tao, L.; Liu, Z.; Zhou, D. Advances in low-field nuclear magnetic resonance technologies applied for characterization of pore space inside rocks: A critical review. *Pet. Sci.* **2020**, *17*, 1281–1297. [CrossRef]
20. Cheng, Z.; Ning, Z.; Yu, X.; Wang, Q.; Zhang, W. New insights into spontaneous imbibition in tight oil sandstones with NMR. *J. Pet. Sci. Eng.* **2019**, *179*, 455–464. [CrossRef]
21. Dai, C.; Cheng, R.; Sun, X.; Liu, Y.; Zhou, H.; Wu, Y.; You, Q.; Zhang, Y.; Sun, Y. Oil migration in nanometer to micrometer sized pores of tight oil sandstone during dynamic surfactant imbibition with online NMR. *Fuel* **2019**, *245*, 544–553. [CrossRef]
22. Lin, Z.; Hu, Q.; Yin, N.; Yang, S.; Liu, H.; Chao, J. Nanopores-to-microfractures flow mechanism and remaining distribution of shale oil during dynamic water imbibition studied by NMR. *Geoenergy Sci. Eng.* **2024**, *241*, 213202. [CrossRef]
23. Zhang, Q.; Dong, Y.; Tong, S. Pore-type-dependent fractal features of shales and implications on permeability. *Fractal Fract.* **2023**, *7*, 803. [CrossRef]
24. Li, G.; Xin, B.; Li, Z. Pore structure characterization and fractal analysis of lacustrine shales: Integrating N_2 adsorption, mercury intrusion, and deep learning-assisted FIB–SEM 3D pore surface point cloud reconstruction. *Fractal Fract.* **2026**, *10*, 179. [CrossRef]
25. Zhao, K.; Zhang, Z. NMR and SEM fractal dimensions explore shale pore structure taking the Upper Paleozoic shale in Ordos Basin as an example. *PLoS ONE* **2025**, *20*, e0323968. [CrossRef] [PubMed]
26. Wu, H.; Kong, X.; Chen, X.; Guan, D. 3-D fracture network reconstruction and quantitative fractal analysis of subsurface rock fractures via integrated CT scanning and box-counting dimension methodology. *Results Eng.* **2025**, *26*, 105614. [CrossRef]

27. Wang, Y.; Zhai, C.; Liu, T.; Sun, Y.; Tang, W.; Wang, J.; Xu, H.; Huang, T. 3D multifractal analysis of explosion-induced fractures in bedding shale using μ-CT imaging. *Eng. Fract. Mech.* **2025**, *324*, 111268. [CrossRef]
28. Zong, P.; Xu, H.; Tang, D.; Chen, Z.; Huo, F. A fractal model of fracture permeability considering morphology and spatial distribution. *SPE J.* **2024**, *29*, 4974–4987. [CrossRef]

Disclaimer/Publisher's Note: The statements, opinions and data contained in all publications are solely those of the individual author(s) and contributor(s) and not of MDPI and/or the editor(s). MDPI and/or the editor(s) disclaim responsibility for any injury to people or property resulting from any ideas, methods, instructions or products referred to in the content.